Numerical Study on the Formation Mechanism of the Arid Climate in Northeastern Asia

A Dissertation Submitted to
the Graduate School of Life and Environmental Sciences,
the University of Tsukuba
in Partial Fulfillment of the Requirements
for the Degree of Doctor of Philosophy in Science

Tomonori SATO

Abstract

Formation mechanism of the arid climate in northeastern Asia is investigated using a regional climate model. Two kinds of long-term numerical experiments are carried out with a real topography and with a modified topography which does not contain the TianShan and the Altai Mountains. Simulated rainfall distribution with the real topography shows maximum precipitation over upwind slope of the mountain and minimum precipitation in downwind side of it, which is consistent with the feature of rain-shadow in other regions of the world. However, numerical experiment without the TianShan Mountains also simulates the area of distinct minimum precipitation in the same location. This leads that the arid climate is formed even though the rain-shadow effect is absent. The difference in rainfall amount between these two experiments is very small around the downwind side characterized by the arid region. On the other hand, more intense and frequent rainfall events tend to occur in upwind side of the mountain range due to forced lifting of environmental flow, which just emphasizes the contrast in rainfall distribution between upwind and downwind side of the mountain. Regardless the TianShan Mountains exists or not, the subsidence prevails over the arid region in summer, and suppresses precipitation when synoptic scale disturbances are situated in vicinity of the desert region.

Sensitivity of the subsidence prevailing over the arid region during summer is investigated by regional climate model experiments. An experiment without diabatic heating shows very gentle vertical motion over the arid region, which indicates that the mechanical effect of the Tibetan Plateau is not enough to cause the subsidence. On the other hand, the subsidence is strongly enhanced in case that the diabatic heating processes, such as radiation and condensation, are added in the model. Additionally, horizontal and vertical structures of vertical motion are very similar even when diabatic heating by only radiation process is included in the model. The elevated ground surface of the mountainous region, especially the Tibetan Plateau, is heated in the model as a result of solar radiation inducing large sensible

heat flux. Atmospheric circulation around the East Asia should be strongly influenced by the elevated heat source. Previous studies mainly focuses on the relationship between the aridity in middle latitude Asia and diabatic heating over the tropical regions since vertically integrated diabatic heating rate is larger in tropical regions than over the Tibetan Plateau. In this study, further sensitivity experiments assuming an artificial heating over the Tibetan Plateau are conducted in order to study the thermal effect of the Tibetan Plateau on the subsidence. The simulated feature of vertical motion is very similar with that by full diabatic heating model showing distinct subsidence over the arid region. Hence, the diabatic heating over the plateau is crucially important to cause the arid climate in northeastern Asia.

The stationary wave driven by diabatic heating over the plateau tends to propagate northward during boreal summer, since subtropical westerly jet locates north of the plateau. Consequently, precipitation is suppressed by the stationary descending motion around the arid region in northeastern Asia, which is caused by the interaction between zonal wind and diabatic heating over the Tibetan Plateau.

Key words: *arid climate, northeastern Asia, rain-shadow, Tibetan Plateau, diabatic heating, regional climate modeling*

Contents

List of Figures

List of Tables

1. Introduction

1.1. Arid climate in northeastern Asia

Arid climate covers broad extent over land areas where precipitation amount is very small and over oceans with cold currents. Figure 1.1 shows the global distribution of annual precipitation climatology[1]. Over the ocean, arid climates are found corresponding to the cold ocean currents around California Current, Canaries Current, Humboldt Current, Benguela Current, and West Australian Current. Over land, major aridity areas can be found in the Sahara, Kalahari, Australian Desert, Arabian Desert, Iranian Desert, Turkestan Desert, Taklamakan, Gobi, North American Desert, and Atacama. Since the geographical distribution of aridity, in particular deserts, has strongly limited the human activity in historical times, these deserts deserve to investigate their nature and formation mechanisms.

The study area includes the two of the largest desert regions in Asia of the Taklimakan and the Gobi deserts (Fig. 1.2). Both regions can be regarded as part of subtropical arid climate in Eurasian continent extending from the Arabian Peninsula, Central Asia, northern China, and Mongolia. Figure 1.3 shows the spatial distribution of land cover over Asia provided by the U. S. Geological Survey (USGS). Arid region categorized as desert type covers large portion of northwestern China, especially around the Taklimakan desert and the Gobi desert and some parts of southern Mongolia. Semi-desert region distributes surrounding the desert type, that is, western Tibetan Plateau, the Lake of Balkhash in Kazakhstan, and southern half of Mongolia. Short grass type can be found in eastern and northern half of Mongolia and elevated mountainous regions such as the TianShan Mountains and the Altai Mountains. In general, vegetation cover is strongly affected by annual precipitation as well as average temperature. Figure 1.4 shows the annual precipitation distribution in the study area during 1979 and 2001 using GPCP dataset. It is evident that the desert and semi-desert

---

[1] Based on Global Precipitation Climatology Project (GPCP) version 2 dataset (Adler et al., 2003).

climates correspond well to the dry region where annual precipitation less than 100 mm.

Figure 1.5 illustrates the climatology of monthly precipitation in Asia during 1979 and 2001 using GPCP dataset. Horizontal component of the vertically integrated water vapor flux using NCEP/NCAR reanalysis (Kalnay et al., 1996) is also drawn in the figure. In January, monthly precipitation is less than 10 mm over whole the Tibetan Plateau and the Mongolian Plateau, and the water vapor transport is very small in these region (Fig. 1.5a). Whereas, relatively large precipitation rate is observed in Central Asia around the Caspian Sea and the Aral Sea resulting in the wettest season in this region. The rainfall amount is very different between the west and east of the dividing mountain ranges such as the TianShan Mountain, the Altai Mountain, and the Sayan Mountain. Monthly precipitation is larger than 20 mm in the west of those mountain ranges, while the monthly precipitation is nearly zero in the east of them. The area of the dry region, in respect with precipitation rate less than 10 mm $month^{-1}$, becomes gradually small and limited in the desert and semi-desert region in April (Fig. 1.5b). The water vapor transport exhibits larger amount at the same time. In spring, northern China and southern Mongolia becomes most prominent season of the dust storm events (Kurosaki and Mikami, 2002) because synoptic scale disturbances are often passing through this region after the disappearance of the cold winter anticyclone over the northern Asia. Precipitation rate over the arid region increases after April, and it reaches the highest in July in most part of northeastern Asia (Fig. 1.5c). To the contrary, in central Asia, the rainfall rate is being less than 10 mm $month^{-1}$ causing a considerable aridity. In northeastern Asia, large portion of annual precipitation occurs during warm season, whereas annual precipitation is contributed mainly by wintertime precipitation in Central Asia. Such features of the seasonal variability of precipitation have also been described in Yatagai and Yasunari (1995). Figure 1.6 illustrates annual precipitation and the contribution of summertime precipitation based on the rain gauge observation records. As mentioned above, annual precipitation is less than 50 mm in the Taklimakan desert, and around 100 mm in the Gobi desert; but more than half portion of annual precipitation is observed as summertime rainfall. On the other hand, annual precipitation in Central Asia has a minimum with less than 200 mm, and found that the

contribution of the summer precipitation is blow 10 %. The characteristic differences in seasonal variation indicates that the reasons of the aridity may differ between Central Asia and northeastern Asia, although it may be regarded as unique but large arid region in respect to the annual precipitation.

1.2. Previous study on the arid region formation in East Asia.

Global distribution of arid climate can be classified into several types according to the reason of few rainfall events as described in many literatures such as Houghton (1984). Major desert regions over land are considered to owe to at least one of the following causes.

(1) Located in subsidence arms of Hadley and Walker circulations, where subtropical anticyclones prevail.

(2) Lee of dividing mountain range because humid air flow is blocked and lifted to its condensation level over the upwind slope finally causing rainfall there; as a result, less humid air is transported to leeside, so called rain-shadow effect. (Fig. 1.7)

(3) Apart from water resources of ocean.

(4) Inactive synoptic disturbances owing to the stationary Rossby wave, which can be seen around large scale mountains.

In general, most of arid areas on the Earth locate in subtropical regions due to the cause (1). The high pressure belt near 30° latitude is known as prevailing subsidence motion because this belt is situated between the active convection in ITCZ (Inter-Tropical Convergence Zone) and stable ascent associated with mid-latitude storms. Figure 1.7 illustrates a schematic diagram of the "rain-shadow effect" as assigned by cause (2). The physical barrier of the moisture transport by the mountain range has been claimed by many authors describing desert formation processes. The rain-shadow induced desert can be found near lee of large scale mountain or the dividing mountain ranges. For example, Fig. 1.8 shows annual precipitation in the island of Hawaii. Local minimums are prominent in west side of the mountain peak since easterly trade wind prevails in this region. Figure 1.9 also shows the example of rain-shadow

which is observed along longitudinal transect in North America. Annual precipitation clearly decreases in the lee of the dividing mountain ranges.

The desert region in northeastern Asia is located in relatively higher latitude compared with other major deserts within subtropical zone, e.g. the Sahara and interior of the Australian continent. The fact indicates that the Hadley circulation is only little related with the formation of the aridity. As mentioned by Manabe and Broccoli (1990), absence of rain-inducing disturbances is indeed prominent in winter; however it would contribute slightly to the summer dryness because zonal wind velocity is relatively weaker in summer. Previously suggested reasons for the warm season dryness can be summarized as the combination of above mentioned cause (2) and cause (3) in general (Houghton, 1984; Hartmann, 1994; Shinoda, 2002). Recently, hydrological cycle over land becomes a very important theme to understand the global hydrological regime. In particular, water recycle is one of the interesting issues over arid region in mid-latitude Asia. Bosilovich and Schubert (2002) studied the roles of hydrological cycle over land by showing a contribution from evaporation at the land surface to the annual precipitation, and suggested that very small fraction of rain water is originated from ocean in many desert regions in the world. In northeastern Asia, more than 80 % of rain water owes to the evaporation from land surface. The result indicates possible connection between the distance from the ocean and arid climate distributions. However, the contribution from evaporated water is known to show another value depending on the method of analysis (Trenberth, 1999). Additionally, some GCM (General Circulation Model) experiments, for example Manabe and Terpstra (1974) and Manabe and Broccoli (1990), have shown almost annular distribution of rainfall in the model in case that any mountains on the globe were absent. Thus, the distance from the ocean is not always selected reason which can answer why the arid region is located in the current location.

As it can be seen in Fig. 1.10, the desert regions are surrounded with the TianShan and the Altai mountain ranges except for the east side of them. The elevations of these mountain ridges exceed 2000 m. In particular, the peak of the TianShan Mountains is higher than 7000 m which influence on the precipitation systems considerably. Observed annual

precipitation is larger than 300 mm in the west, and smaller than 100 mm in the east of the mountain range. Such a characteristic rainfall distribution is one of the only evidence which supports the importance of rain-shadow effect in this area because only observational inferences were achieved so far concerning propriety of the rain-shadow effect. Compared with schematic figure of rain-shadow in Fig.1.7, upwind of the mountain, Central Asia is never humid as mentioned in section 1.1. Therefore, the influences of rain-shadow effect on this region are not adequately clear even though it has been believed very important as a principal reason of desert formation. In addition, during summer, land-sea heating contrasts over the Asian monsoon region widely modify the atmospheric circulation, and forms quite different system from that in wintertime. Tanaka et al. (2004) attempted the quantitive estimation of the contribution of Hadley, Walker and monsoon circulation to the global divergent field suggesting relatively large contribution from monsoon circulation in boreal summer. Rodwell and Hoskins (1996) suggested the monsoon-desert mechanism to explain the aridity mechanism in the Mediterranean Sea and Central Asia. They concluded that huge diabatic heating originated from deep convection over the South Asia remotely causes the aridity interacting with the mid-latitude westerly. However, they did not consider the role of the Tibetan Plateau as an elevated heat source which was elucidated by many recent works based mainly on observational and analytical research (He et al., 1987; Ueda et al., 2003; Wu and Zhang, 1998; Minoura et al., 2003). Luo and Yanai (1983) found the intense ascending motion over the Tibetan Plateau and descent over the Great Indian Desert (Fig. 1.11). They further suggested that descent motion prevails over the north of the Tibetan Plateau on the 40-days mean basis (Fig.1.12). Many observational efforts have come to reveal the environmental circulation around the Tibetan Plateau. Nevertheless, they do not prove the role of the Tibetan Plateau on the aridity as well as the rain-shadow effect since they just describe the circumstance evidences.

1.3. Purpose of the study

As mentioned above, the formation mechanism of the arid climate in northeastern Asia is still matter of debate regarding the influences of topography. Additionally, no investigations have achieved to clarify the thermal effects of the Tibetan Plateau on the arid climate although many observational and analytical researches have described the detail structure of the heating over the plateau. Thus, this study aims to reconsider and to clarify the formation mechanism of the arid climate, mainly with respect to summertime precipitation, by series of sensitivity experiments using a regional climate model (RCM).

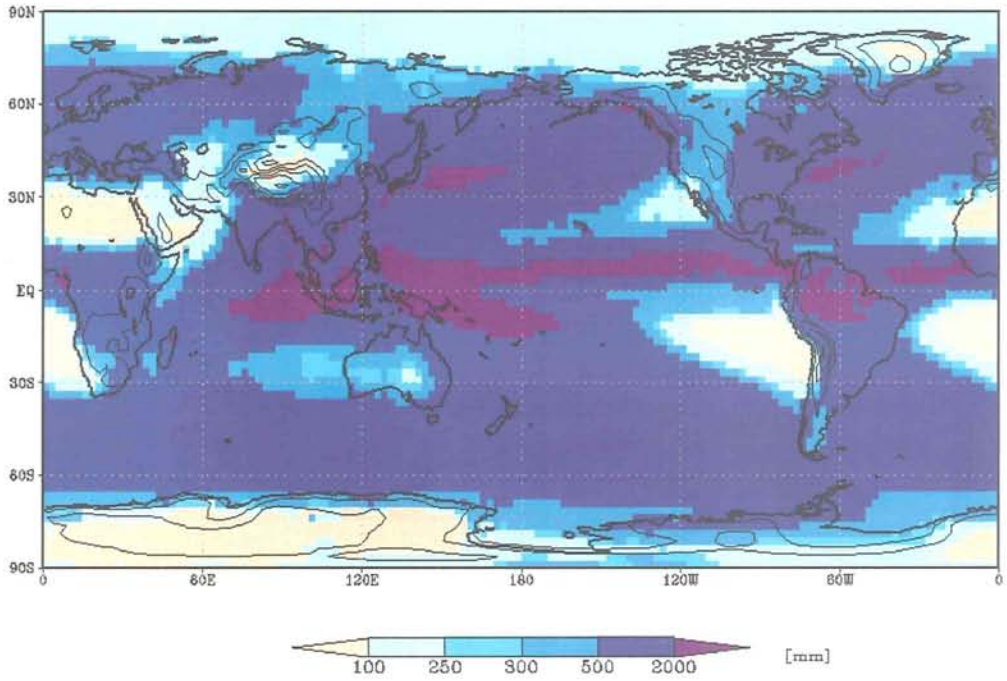

Fig. 1.1: Annual Precipitation climatology (1979-2001) based on the GPCP version 2 dataset (Adler et al., 2003).

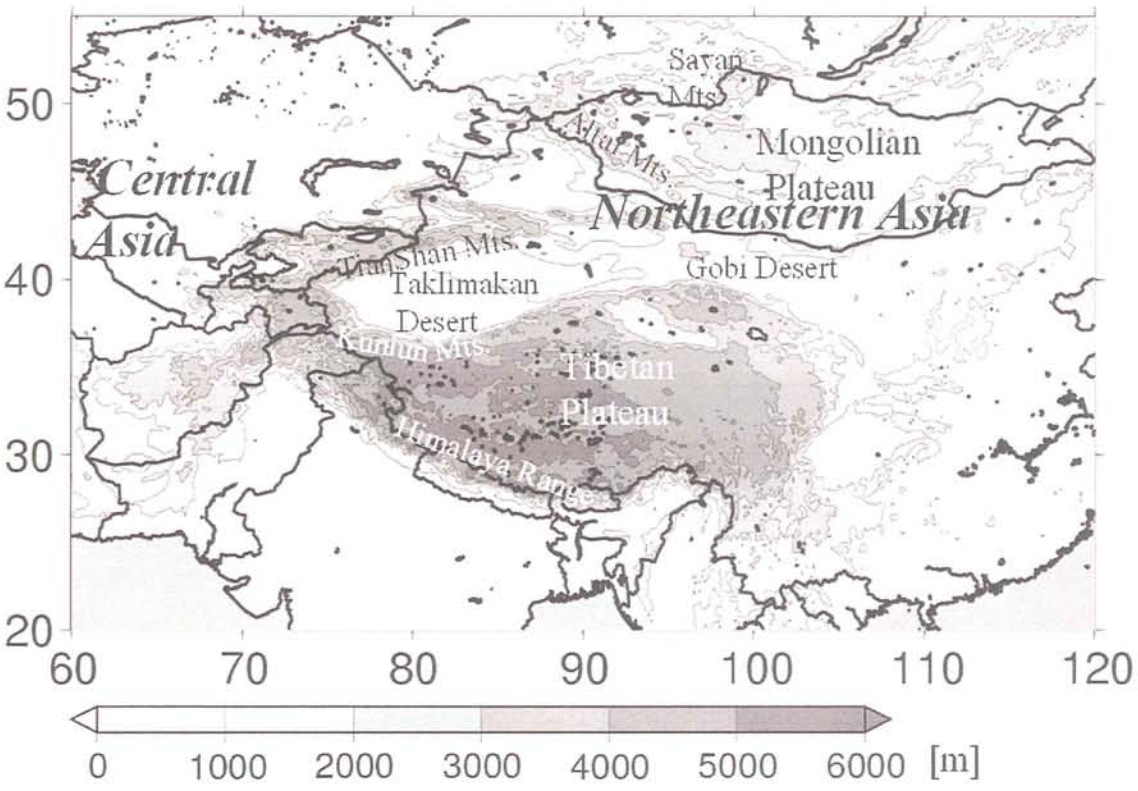

Fig. 1.2: Study area.

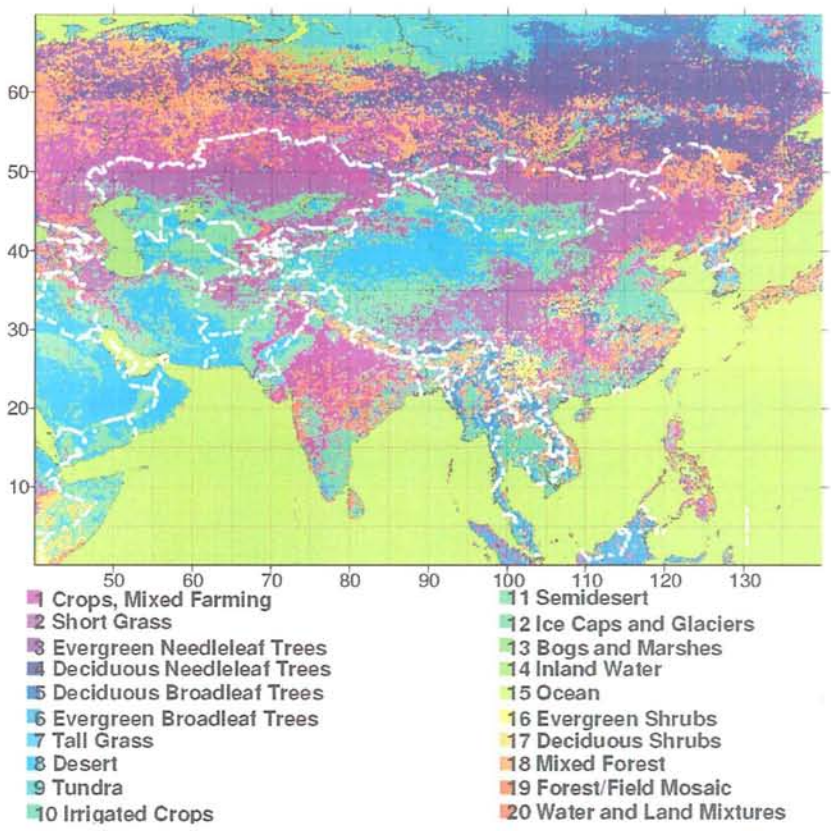

Fig. 1.3: Land cover distribution over Asia. Global land cover characterization dataset provided by USGS is used.

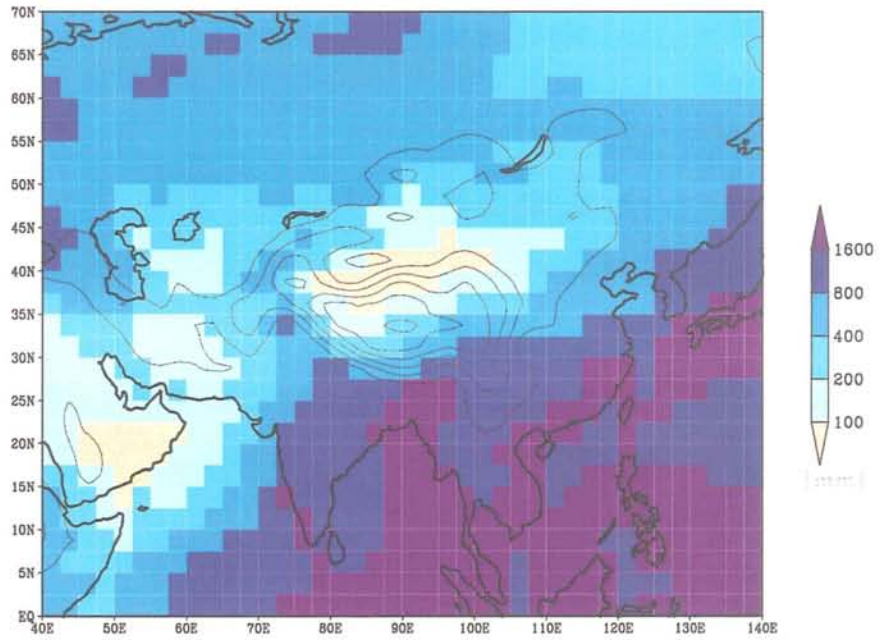

Fig. 1.4: Annual Precipitation climatology around study area (1979-2001). Solid contours indicate topography in 1000 m interval.

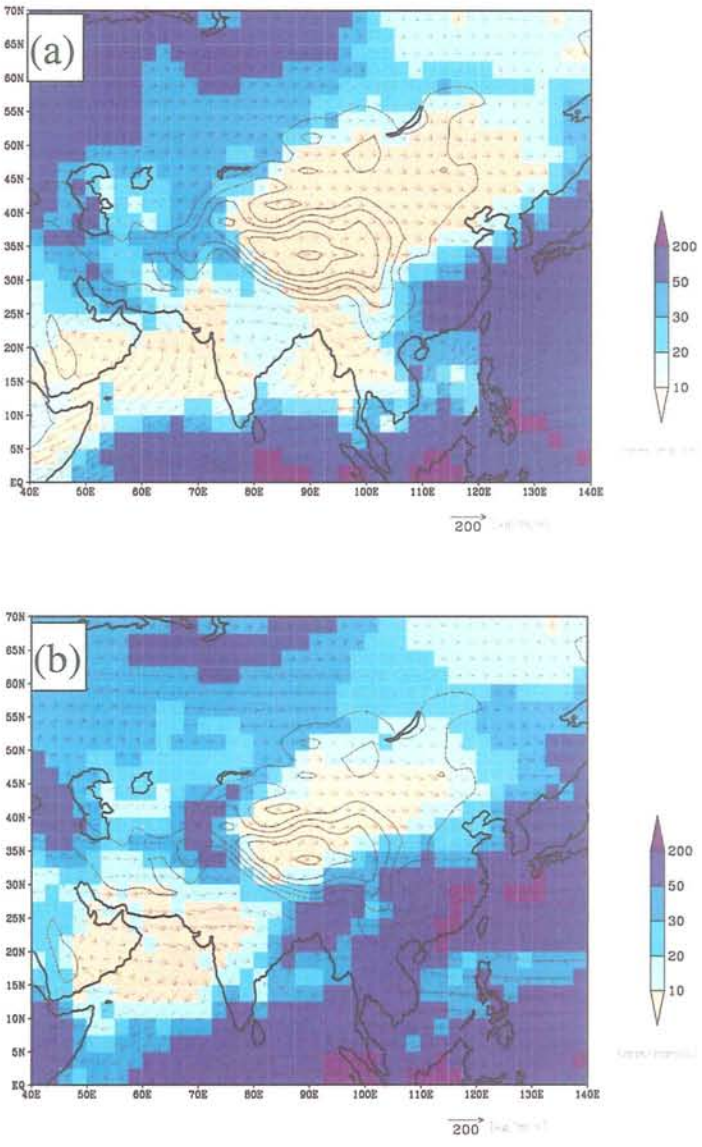

Fig. 1.5: Monthly precipitation climatology (1979-2001). Solid contours indicate topography in 1000 m interval. (a) January, (b) April

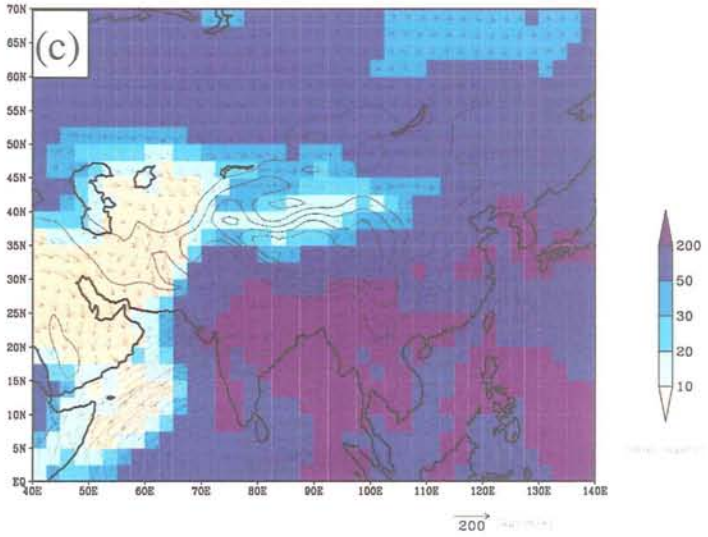

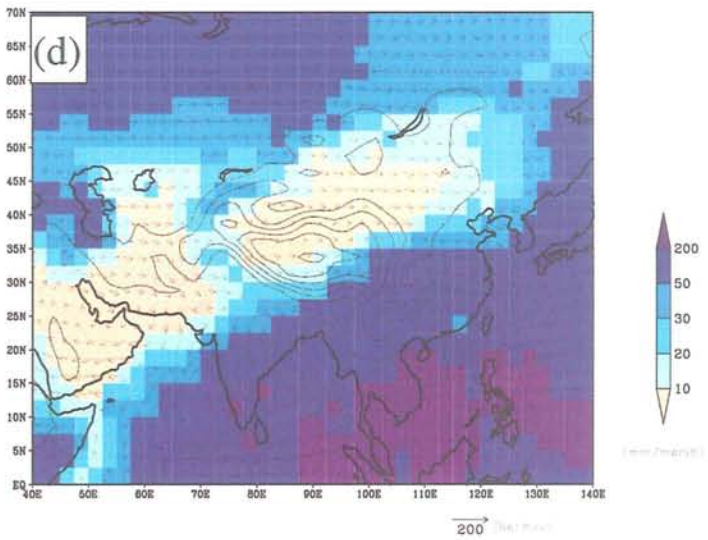

Fig. 1.5: Continued. (c) July, (d) October

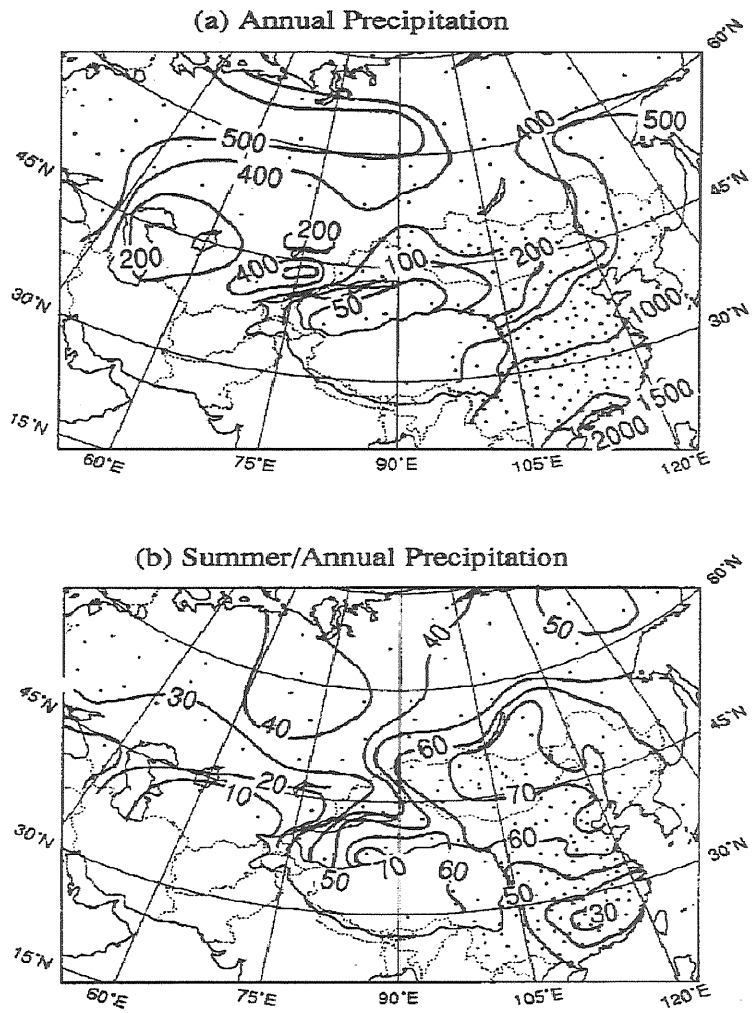

Fig. 1.6: (a) Annual precipitation and (b) the ratio of summertime precipitation to annual precipitation. (From Yatagai and Yasunari, 1995)

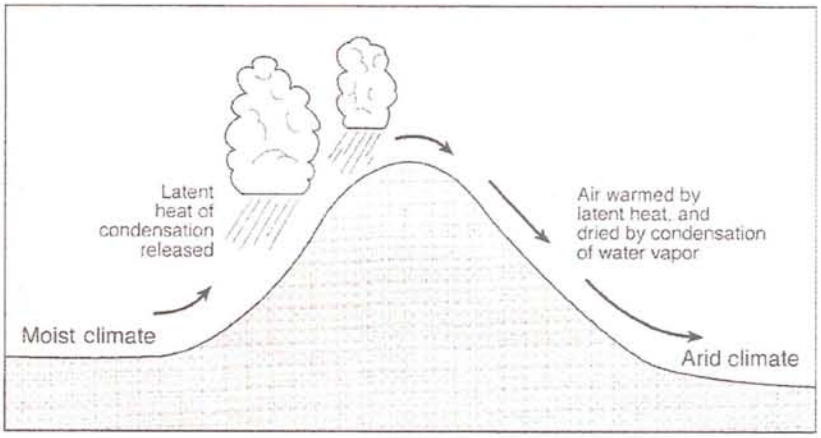

Fig. 1.7: Schematic illustration showing the rain-shadow effect. (From Warner, 2004)

Fig. 1.8: Annual average rainfall over the island of Hawaii. (From Armstrong, 1983)

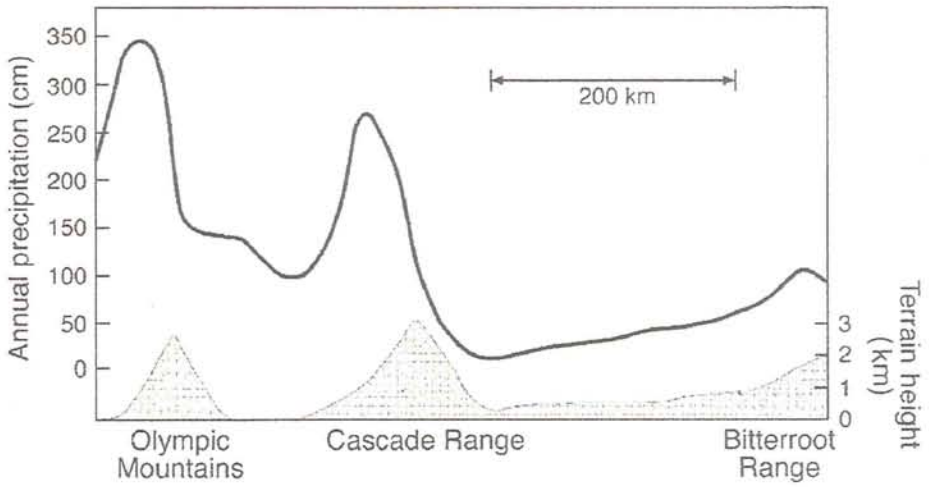

Fig. 1.9: Annual precipitation along an east west line between the Washington. (From Neuberger and Cahir, 1969)

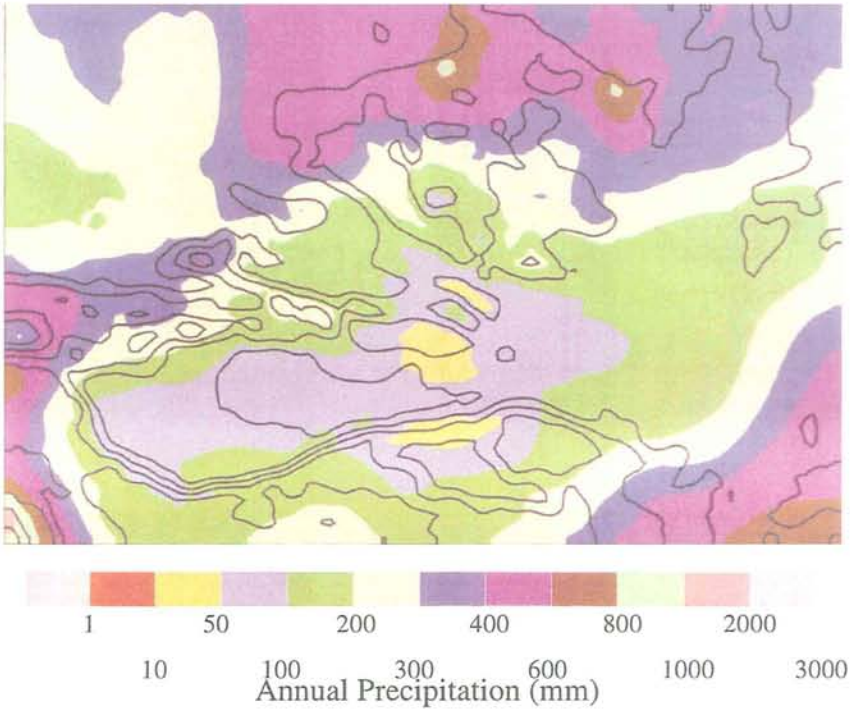

Fig. 1.10: Annual precipitation over northwestern China. (After Warner, 2004). Data based on New et al. (2000). The Taklimakan desert is roughly corresponding to the region with less than 100 mm.

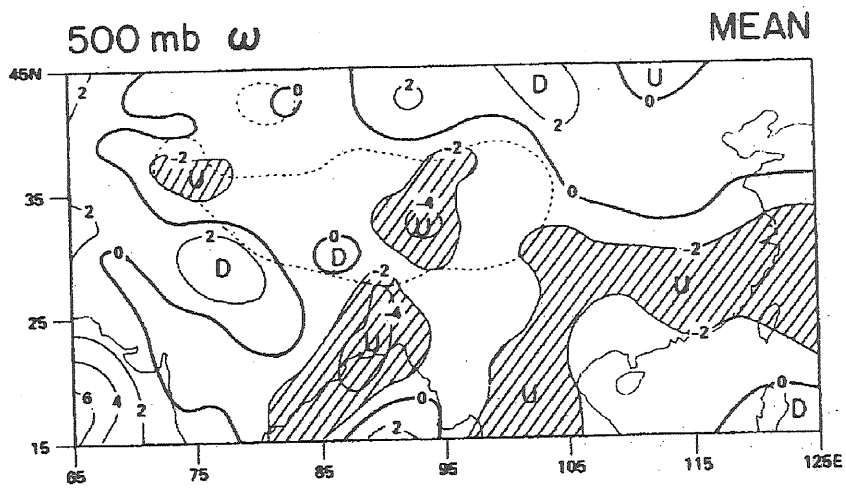

Fig. 1.11: 40-day mean vertical p-velocity (hPa hr^{-1}) at 500 hPa. (From Luo and Yanai, 1983)

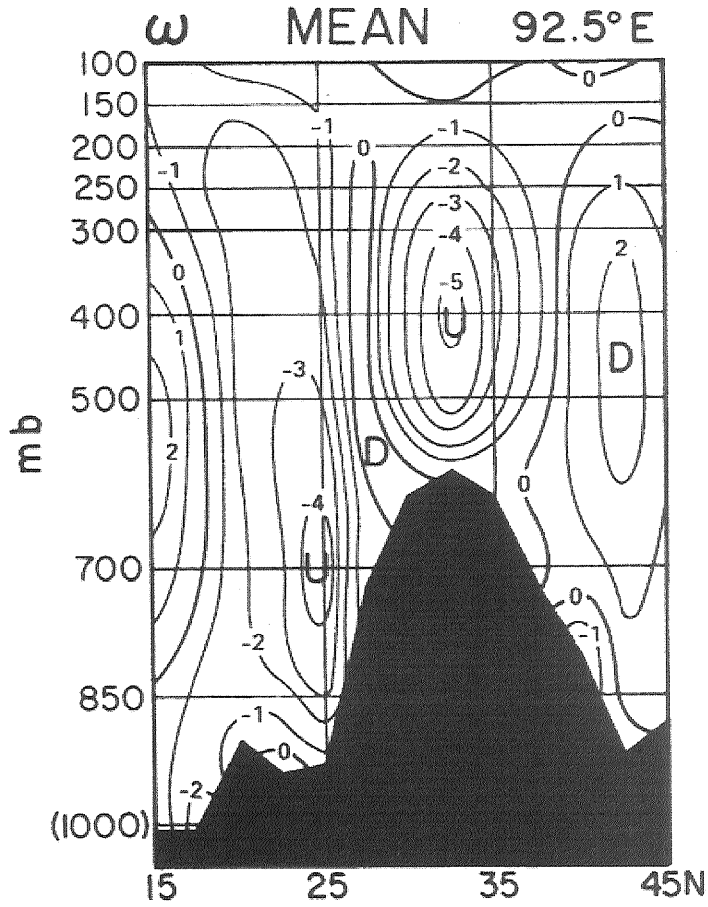

Fig. 1.12: North-south vertical cross section showing the 40-day mean vertical p-velocity (hPa hr^{-1}) along 92.5°E. (From Luo and Yanai, 1983)

2. Methodology

2.1. Numerical Model

The numerical model adopted in this study is the TERC-RAMS (Terrestrial Environment Research Center - Regional Atmospheric Modeling System; Sato and Kimura, 2003; 2005). The original RAMS (The Regional Atmospheric Modeling System) was developed at Colorado State University (Pielke et al., 1992). Physical parameterizations utilized in this study are summarized in Table 2.1. In TERC-RAMS, radiation scheme was replaced by Nakajima et al. (2000), calculating the short wave and long wave radiation in every hour. Cumulus convection scheme was also replaced by Arakawa and Schubert (1974). The number of horizontal grid is 80 x 60 with 150 km grid spacing centered at 85°E and 30°N, so that most part of the eastern Eurasia is included in the model domain. The vertical grid interval is 110 m in the lowest layer, and it gradually stretches up to 900 m in the upper layer. The reanalysis data provided by NCEP/NCAR (Kalnay et al., 1996) were used as an initial condition of the simulation. Monthly mean sea surface temperature data of the Optimum Interpolation Sea Surface Temperature Version 2 (OISSTv2) data (Reynolds et al., 2002) provided by NOAA is used for the surface boundary condition for the ocean. Vegetation type over land is assumed to be short grass all over the model domain for simplicity. The model has 11 soil layers below the ground with 0 cm, 5 cm, 10 cm, 18 cm, 30 cm, 50 cm, 70 cm, 90 cm, 120 cm, 150 cm and 180 cm depth. Initial soil moisture is assumed to be horizontally homogeneous with 0.6 of volumetric water content above 50 cm, and increases to 1.0 in the deepest layer. The advantage to use RCM is an ability to carry out the idealized sensitivity studies rather than the higher spatial resolution. Several sensitivity experiments are carried out by this model as listed up in Table 2.2, and they are addressed in next section.

2.1. Long-term integration (LT-CTL and LT-NoM)

First of all, the role of the mountain range, such as the TianShan, the Altai and the Sayan, as a barrier of the precipitation system, that is rain-shadow effect by surrounding mountains, is investigated by two kinds of long-term integrations by the climate model. The first experiment, referred to as long-term control run (LT-CTL), simulates realistic atmospheric circulation and precipitation using six-hourly reanalysis data as boundary condition. In another sensitivity experiment, referred to as long-term no mountain run (LT-NoM), not only the TianShan Mountains but also any topography over Mongolian plateau is assumed to be flat with 500 m elevation. Topography used in both experiments is illustrated in Figure 2.1. Note that the both LT-CTL and LT-NoM experiments are basically same except for the topography. Outputs of these simulations are analyzed after five days spin-up period. The prognostic variables in the lateral boundary are nudged to the reanalysis data with a linear nudging coefficient. Whereas, the TERC-RAMS itself calculates the meteorological elements without reanalysis data over most of the model domain except for the boundary. Numerical integration of each experiment is carried out for ten years of July from 1991 to 2000.

2.2. Zonal mean experiments

As mentioned above, one of the large advantages to use RCM is its capability of characteristic experiments conducted by ideal boundary conditions. In this study, zonal mean field is adopted as a boundary condition of the numerical model. Such experiment makes it possible to investigate the impact of the zonal mean component of the atmosphere on the certain climate processes, for example, formation mechanism of the arid climate. The concept of this integration is very similar to previous study by Yoshikane et al. (2001) which clarifies the formation mechanism of the Baiu front in eastern Asia. Zonal averaged sea surface temperature calculated using OISSTv2 is also applied in zonal mean experiments.

2.2.1. ZM-CTL experiment

In a ZM-CTL (zonal mean control) experiment, initial and boundary conditions are replaced by a global zonal mean values during July of 2000 calculated using the NCEP/NCAR reanalysis data (Fig. 2.2). Since boundary variables are fixed during the numerical integration, most of the synoptic disturbances passing into the model boundary can be neglected. According to this, the circulation pattern induced by surface inhomogeneity, i.e., orography and ocean-land contrast, and zonal flow itself will be the most dominant factor in the ZM-CTL experiment. After 30 days integration, the averaged values during only last ten days, during day 21 to day 30, are analyzed in a similar manner as Yoshikane et al. (2001).

2.2.2. ZM-NoC and ZM-NoR experiment

Condensation process plays an important role in atmospheric circulation during warm season, because it widely modifies the energy balance as a result of change in water phase. The sensitivity of the latent heat release is examined in an experiment, referred to as ZM-NoC, (Zonal Mean – No Condensation) by turning off the condensation process in the model without any other changes from the ZM-CTL experiment. The Tibetan Plateau may still act as an elevated heat source even if no condensation occurs in the ZM-NoC experiment, because the plateau is directly heated by the solar radiation. Another sensitivity experiment, referred to as ZM-NoR (Zonal Mean – No Radiation), which is same as ZM-NoC but excludes the radiation process, is carried out in order to simulate only mechanically forced flow passing over and around mountain like Rossby waves and mountain waves. The ZM-NoR experiment is the simplest experiment in this study which only calculates the adiabatic process of the climate system in a zonal mean environment.

2.2.3. ZM-TbQ experiment and ZM-SAQ experiment

As addressed in Section 1.2, many observational studies have suggested the existence

of descending motion over the arid region as well as prominent upward motion over the Tibetan Plateau. However, they could never reveal the source of the subsidence, for example mechanical effect, thermal effect, or more large-scale interaction, although some possible effects by the Tibetan Plateau was somewhat implied. The difficulty to determine the source of subsidence owes to the existences of complex topography in East Asia and large diabatic heating rate in South Asia rather than the existence of the Tibetan Plateau itself.

The ZM-TbQ experiment is conducted in which artificial heat source is given on the ZM-NoR experiment. The heat source is placed only over the Tibetan Plateau in order to study the impact of diabatic heating of the plateau. The area of the heat source is defined by the ground altitude exceeding 3000 m Above Sea Level (ASL). Although vertically integrated diabatic heating rate depends on ground altitude due to adoption of the sigma-z coordinate, it is approximately 160 W m^{-2} over the plateau, whose magnitude does not conflict with the previous observational study by Yanai and Li (1994). The vertical structure of the heat source is distributed between ground surface and about 6500 m ASL.

Rodwell and Hoskins (1996) analyzed a global distribution of diabatic heating rate using reanalysis data. Deep convection often occurs around the Bay of Bengal and over the Indochina Peninsula causing a large diabatic heating in this region. In order to study the relationship between the diabatic heating and arid climate formation, ZM-SAQ experiment is conducted assuming an artificial heat source over South and Southeast Asia region in the same manner with ZM-TbQ experiment.

2.2.4. ZM-AQUA and ZM-FLQ experiment

The atmospheric response to the heat source is likely to be disturbed by the mechanical forcing of the topography, since East Asia includes very complex terrain such as the Tibetan Plateau and surrounding mountains around the arid region. The ZM-FLQ experiment simplifies the topography with 0 m ASL in calculation domain, in other words, no mountain exists in the whole model domain. Since land-ocean contrast is also possible to disturb the

systematic response to the heat source, surface boundary is assumed to be covered by the ocean in ZM-AQUA. Thus, surface boundary condition of the model exhibits aqua planet which is often attempted by GCMs. Artificial diabatic heating is assumed by the rate of 10 K day^{-1} between surface and 9000 m ASL in location corresponding to the Tibetan Plateau. The heating rate is very large in order to emphasize the effect of diabatic heating. The ZM-FLQ and ZM-AQUA experiments are performed separately for each 12 month of the year, where lateral boundary is assumed to be monthly averaged global zonal mean of meteorological variables in 1998 calculated by NCEP/NCAR reanalysis data for each month. Numerical integration is carried out in 30 days period, and meteorological variables averaged during 21 to 30 days are used for data analysis. Aim of these experiments is to investigate the nature of the heat source response under idealized condition including seasonal variation.

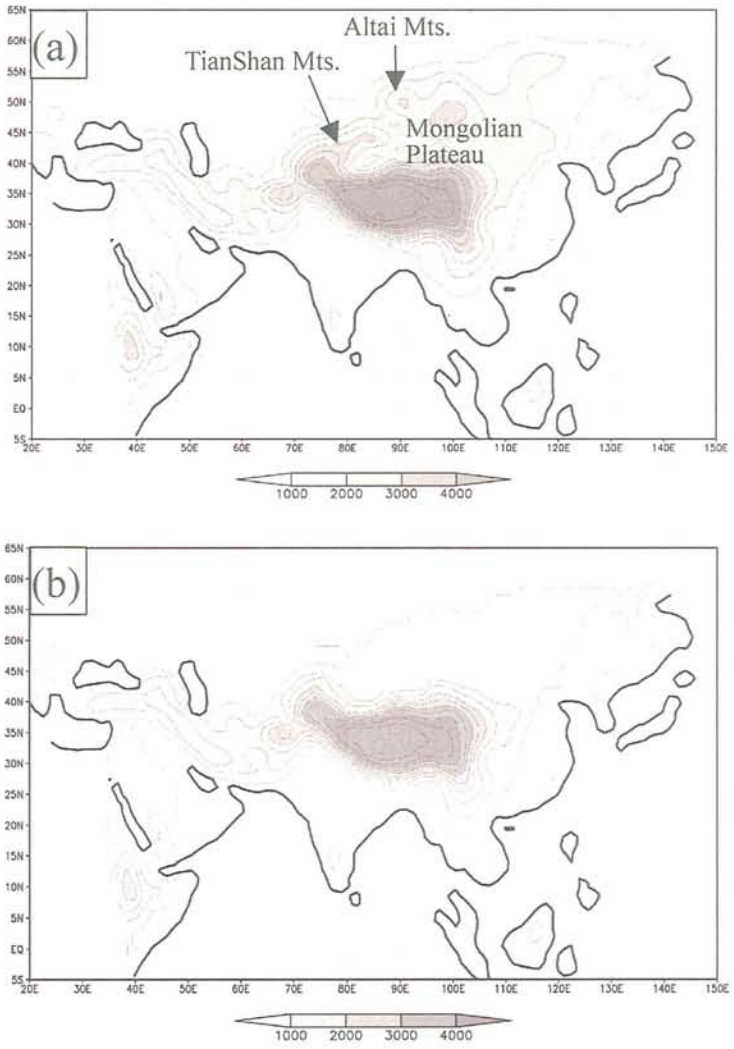

Fig. 2.1: Topography assumed in long term integration. (a) LT-CTL, (b) LT-NoM. Solid contours are drawn in each 500 m.

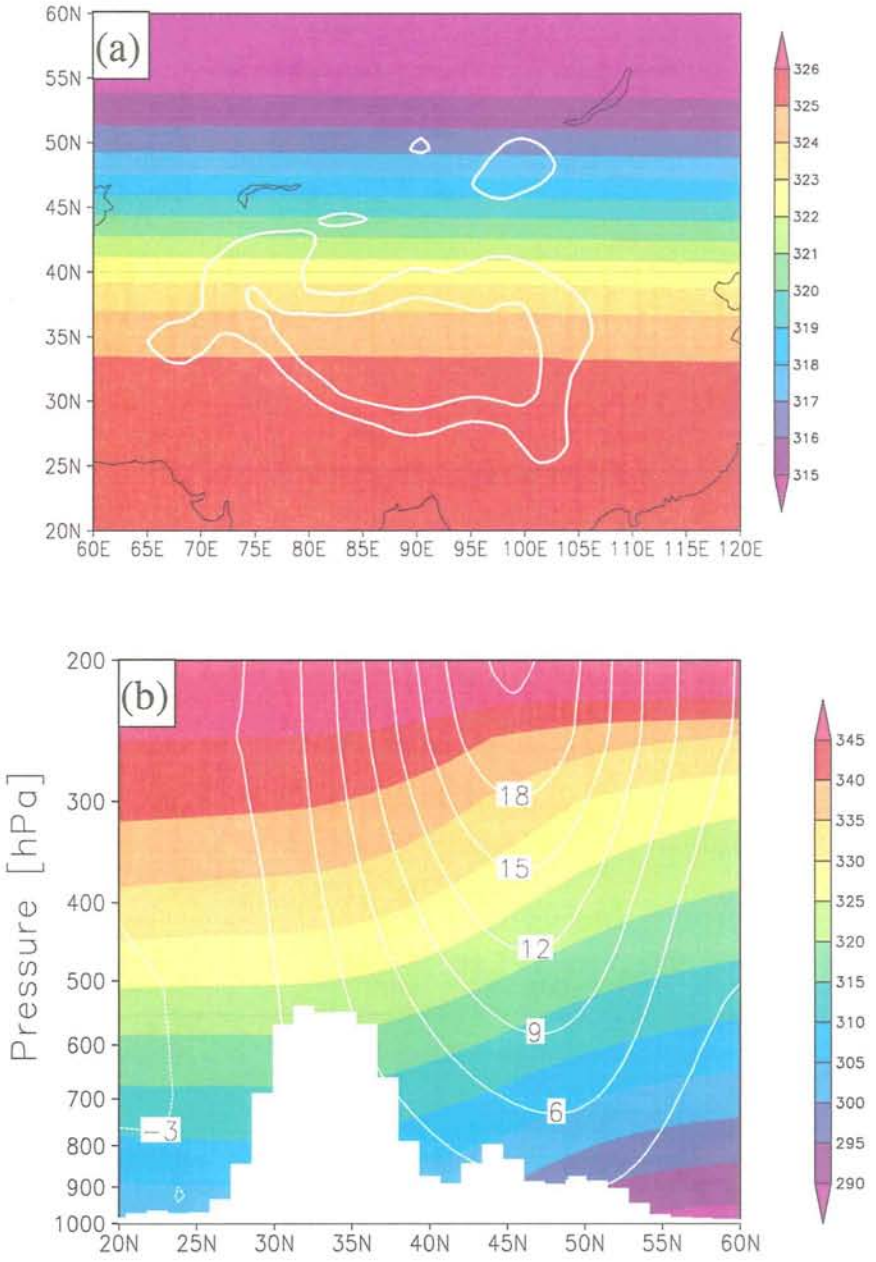

Fig. 2.2: Zonal mean field of July 2000. (a) Potential temperature at 500 hPa. (b) north-south cross section of potential temperature (K) and zonal wind speed (contour; m sec^{-1}).

Table 2-1: List of physical parameterizations and experimental setup

TERC-RAMS
Basic equation and coordinates Compressive non-hydrostatic equations Terrain following vertical coordinate (Z*)
Physical parameterizations Bulk type cloud microphysics (Walko et al., 1995) Cumulus convection (Arakawa and Schubert, 1974) Band scheme radiation (Nakajima et al., 2000)
Horizontal grid system 80 x 60 grid points centered on 85°E, 30°N 150 km grid spacing Vertical grid system 30 layers up to 16 km, 110 m grid interval in lowest layer Soil layer 11 levels with 0 cm, 5 cm, 10 cm, 18 cm, 30 cm, 50 cm, 70 cm, 90 cm, 120 cm, 150c m and 180 cm depth
Boundary condition Lateral and upper boundaries are nudged to NCEP/NCAR reanalysis data (Kalnay et al., 1996) by linear coefficients (see also Table 2.2) SST Monthly mean sea surface temperature of OISSTv2 (Reynolds et al., 2002) Initial soil moisture 0.6 of volumetric water content. Homogeneous vegetation cover: grassland

Table 2-2: List of sensitivity experiments. TP indicates the Tibetan Plateau.

Run name	Boundary	convection	Radiation	remarks
LT-CTL	6-hourly realistic July, 1991-2000	on	on	Realistic topography (Fig. 2.1a)
LT-NoM	6-hourly realistic July, 1991-2000	on	on	Flat Mongolian Plateau (Fig. 2.1b)
ZM-CTL	Time-independent, Global zonal mean of July 2000	on	on	Realistic topography
ZM-NoC	Time-independent , Global zonal mean of July 2000	off	on	Realistic topography
ZM-NoR	Time-independent , Global zonal mean of July 2000	off	off	Realistic topography
ZM-TbQ	Time-independent , Global zonal mean of July 2000	off	off	Realistic topography, Artificial heating on TP
ZM-SAQ	Time-independent , Global zonal mean July 2000	off	off	Realistic topography, Artificial heating on South and Southeast Asia
ZM-FLQ	Time-independent , Global zonal mean of January-December, 1998	off	off	Flat topography, Artificial heating corresponding TP
ZM-AQUA	Time-independent , Global zonal mean of January-December, 1998	off	off	Aqua planet , Artificial heating corresponding TP

3. Rain-shadow effect induced by the TianShan Mountains

3.1. Rain-shadow and the arid region

Figure 3.1 illustrates ten-year mean of monthly precipitation and vertically integrated water vapor flux simulated in LT-CTL experiment. The region of remarkable aridity, around which rainfall is less than 20 mm, is produced in northern China (85°E, 44°N). This region corresponds well with the Taklimakan desert, although it exists slightly north compared with real location centered around 83°E, 39°N. The feature of simulated precipitation agrees fairly well with observed rainfall distribution in this area (see also Fig.1.5c). The water vapor flux is very small over the entire Mongolian Plateau because precipitable water vapor is relatively small due to high elevations. Water vapor transported into the arid region is mainly originated from west of the mountain ranges according to a prevailing westerly wind. The amount of water vapor flux retains 100 kg m^{-1} sec^{-1} over western part of the TianShan Mountains which converges in upwind slope of the mountain. As a result, the rainfall exceeds 80 mm in upwind side of the mountain ranges. On the other hand, the amount of water vapor transported into the arid region is very small, and the region of minimum precipitation also corresponds to that of the maximum divergence of water vapor transport (Fig. 3.3). The features of water vapor flux and rainfall distribution are similar with other rain-shadow induced aridity in the world, such as lee of mountain peaks in North America (Fig. 1.9). The rain-shadow effect seems to be very important to form the arid region in northeastern Asia as long as rainfall distributions by LT-CTL run and by previous observational studies are demonstrated.

Figure 3.2 shows ten-year mean of monthly precipitation in LT-NoM experiment. Topography is drawn by solid contours, in which not only the TianShan Mountain but also any other mountains do not exist in Mongolian Plateau. By comparison with Fig. 3.1, the amount of water vapor flux is larger over whole Mongolian Plateau than that in LT-CTL run since the

precipitable water vapor is relatively larger in LT-NoM run due to the lower elevations. Nevertheless, very similar rainfall distribution with LT-CTL run is obtained in LT-NoM run in respect with the position of arid region. The arid region is well corresponding to the divergence of water vapor flux as seen in Fig. 3.4. This means that the arid region, in which rainfall is less than 20 mm, is formed in the same location with LT-CTL run even though the TianShan Mountain is absent. In addition to the rain-shadow effect, other mechanisms should be considered to explain the formation of arid region in LT-NoM run. Over the Kunlun Mountain, increase of the precipitation is prominent since moist air flow associated with synoptic scale disturbances tends to be directly uplifted over the mountain slope.

Figure 3.5 shows a plot of monthly precipitation across the TianShan Mountains along the line as shown in Fig. 3.1. Obvious peak appears over upwind western slope of the mountain in LT-CTL run as a result of a forced lifting of the environmental flow by the terrain. Then, precipitation decreases rapidly over the mountain top, showing a minimum over downwind slope. On the other hand, precipitation in LT-NoM run decreases smoothly with a minimum value around 85°E because the topography is assumed to be flat as shown with dark shade in the figure. Amounts of minimum precipitation is about 1.5 times larger in LT-NoM run compared with LT-CTL run, although they are basically very small in both runs. From this point of view, the major difference between LT-CTL run and LT-NoM run is restricted in more westerly than 85°E. Therefore, the TianShan Mountains hardly affects the aridity in its leeside, while it contributes largely to the increase of rainfall in upwind slope. In other words, upwind side of the mountain can become humid owing to the existence of mountain despite that precipitation is basically small in northern China.

Decrease of monthly precipitation in LT-NoM run is apparent in eastern part of Mongolia around 105°E, 48°N (see Fig. 3.1 and Fig. 3.2). The fact indicates that the mountains play an important role to supply rainfall in this area causing interaction with an environmental atmosphere by mechanical and thermal processes. In spite over semi-arid steppes, well developed convective systems are often observed over Mongolia and northern China (Yoshino, 1991; Sato, 2004; Takemi, 1999; Takemi and Satomura, 2000). Results of

LT-CTL and LT-NoM experiments suggest that the roles of mountain slopes to initiate and to develop convective systems are very important to the warm season rainfall in the lee and over mountains in this area. Further analysis using satellite data is addressed in section 5.3.

3.2. Suppression of synoptic scale disturbances

During warm season, rainfall events in the arid region tend to be observed as short-term heavy rainfall (Warner, 2004; Batima and Dagvadorj, 2000). Generations of such convection systems should be deeply related with synoptic scale environment because this region locates in one of the most prominent area in frequency of cyclogenesis in northern hemisphere (Fig. 3.6).

Figure 3.7 illustrates a typical rainfall event simulated during 17 and 20 of July 1995 by LT-CTL run. Contours and arrows indicate geopotential height at 500 hPa and vertical integration of water vapor transport, respectively. The rainfall amount is shown as three-hour accumulation. Figure 3.8 illustrates the same rainfall event but simulated in LT-NoM run. At 12 UTC of 17 July 1995, upper level trough is situated over western Siberia accompanied with well organized rainfall band extending southward (Fig. 3.7a and Fig. 3.8a). As it approaches northern China, relatively large amount of water vapor is transported into the arid region because the interception by the TianShan Mountains does not occur in LT-NoM run (Fig. 3.8b, c), while rainfall enhancement over the western slope of the TianShan Mountains and the Altai Mountain is prominent in LT-CTL run (Fig. 3.7b, c). The banded precipitation, however, becomes partially weaken, and almost vanishes out just over the arid region despite sufficient moisture transports persist in both LT-CTL and LT-NoM run. Then, regeneration of the banded precipitation occurs immediately after the trough passing through the arid region in 12 UTC of 20 July 1995 in LT-NoM (Fig. 3.8d). Most precipitation systems passing in this region are similar to this event regarding the behaviors of rainfall distribution; thus, rainfall amount is particularly small over the arid region. These two experiments indicate that the rain-shadow effect cannot explain the reason why the arid climate extends in current location.

Figure 3.9 and Fig. 3.10 illustrate the north-south cross section of ten-year mean vertical motion along 85°E in both LT-CTL and LT-NoM run, respectively. These two experiments clarifies that distinct descending motion prevails in center and north of the Tibetan Plateau. The descending motion over the plateau is formed as a result of too strong upward motion in northern and southern edge of the plateau corresponded with the Kunlun Mountains and the Himalayas. In north of the plateau, velocity of the descending motion is stronger than 0.5 cm sec^{-1}, and centered around 500 hPa over the desert region. Luo and Yanai (1983) have suggested the existence of descending motion in north of the Tibetan Plateau (Fig. 1.12). The vertical structure of the vertical motion is very close to our experiments. Sato and Kimura (2004) suggested that the diabatic heating over the Tibetan plateau causes a regional scale subsidence over northeastern Asia arid region. The subsidence is very important to form the arid region since the minimum precipitation appeared in northeastern Asia completely follows on this robust subsidence (see also Fig. 3.2). In general, synoptic scale disturbances should contribute large portion of annual and summertime precipitation in mid-latitude region. However, few rainfall events are observed over the arid region according to the regional scale subsidence, which produces the characteristic contrast of precipitation between arid and surrounding regions.

Some positive feedbacks which enhance or sustain arid areas can be considered to play an important role in desert regions. For example, albedo/transpiration feedback (e.g. Charney, 1975) and Soil-moisture feedback (Xue and Shukla, 1993) are suggested to enhance arid climate. In current study, transpiration feedback is neglected due to an assumption of homogeneous vegetation cover. Although the soil-moisture feedback is also neglected initially since initial soil moisture is assumed to be horizontally homogeneous condition, the soil moisture gradually decreases over the arid region during numerical integration owing to few rainfall events, which may cause soil-moisture feedback. However, the simulations prove that the arid climate is formed without initial perturbations inducing positive feedbacks.

The rain-shadow effect induced by the TianShan, the Altai, and the Sayan Mountains is believed to largely decrease the rainfall amount to the east of them. Thus, such process has

been thought to strongly affect the formation of the arid climate before this study; there are many literatures describing the rain-shadow effect as a reason of the aridity (e.g. Werner, 2004; Houghton, 1984). The comparison between LT-CTL and LT-NoM clearly states that the rain-shadow effect by those mountains is never inducing the arid climate in northeastern Asia. The raised process, suppression of the synoptic disturbances by the descending motion and its linkage to the aridity is addressed in next section as well as source of the subsidence.

3.3. Summary

The role of mountain ranges upon the arid climate formation in northeastern Asia is investigated by long-term experiment of regional climate model. Before this study, the rain-shadow effect by the mountains is considered to be a major reason of this arid region. Two kinds of numerical experiments are carried out with real orography and with modified orography which does not contain the TianShan Mountains. The precipitation in LT-CTL run shows the maximum in the upwind side of the mountain range. One may think that the downwind minimum is formed by a rain-shadow effect of the mountain range. However, numerical experiment without the TianShan Mountains simulates the distinct arid region as well. This fact indicates that the arid climate in northeastern Asia is formed even though the rain-shadow effect is absent. The role of the TianShan Mountains is just to increase the precipitation in the upwind side, and the mountain hardly affects the amount of precipitation in the lee side. The regional descending motion tends to prevail in both experiments over the arid region. It is indicated that the precipitation over the arid region is suppressed by the subsidence in both experiments.

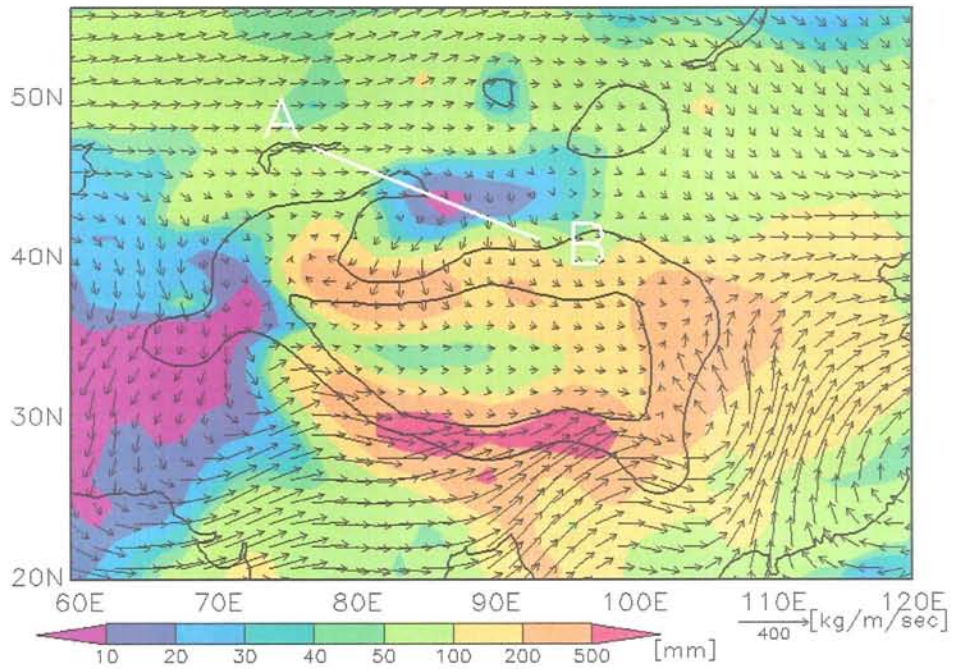

Fig. 3.1: Ten-year mean monthly precipitation and vertically integrated water vapor flux in July by LT-CTL run. Solid contours indicate 2000 and 4000 m of the topography. The line between A and B indicates the cross section shown in Fig. 3.5.

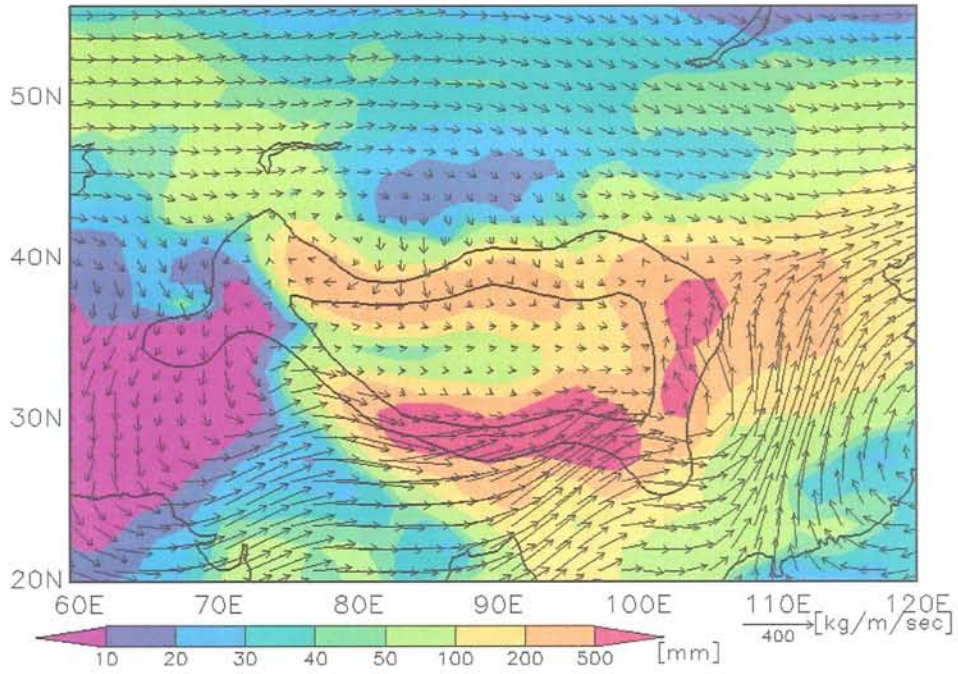

Fig. 3.2: Same with Fig. 3.1 except for LT-NoM run.

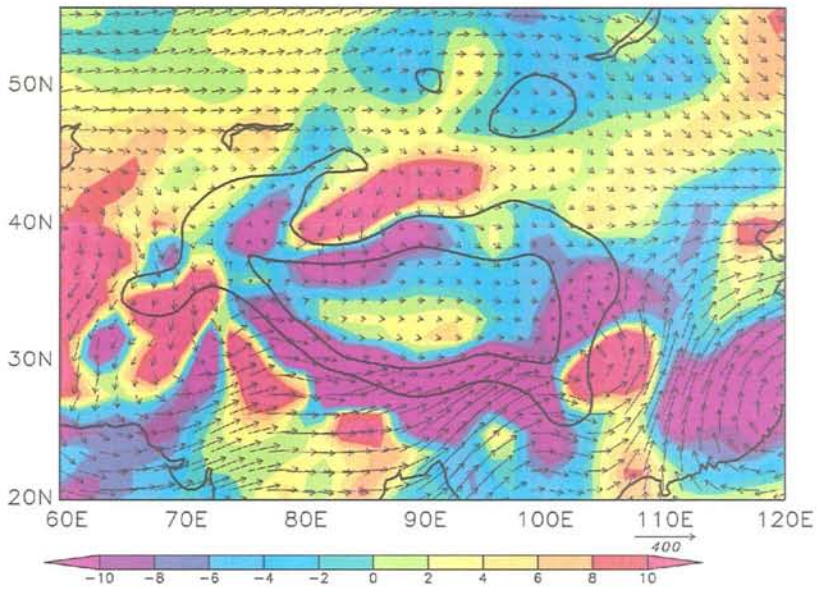

Fig. 3.3: Divergence of ten-year mean water vapor flux (10^4 kg sec^{-1}) and vertically integrated water (kg m^{-1} sec^{-1}) vapor flux in July by LT-CTL run. Solid contours indicate 2000 and 4000 m of the topography.

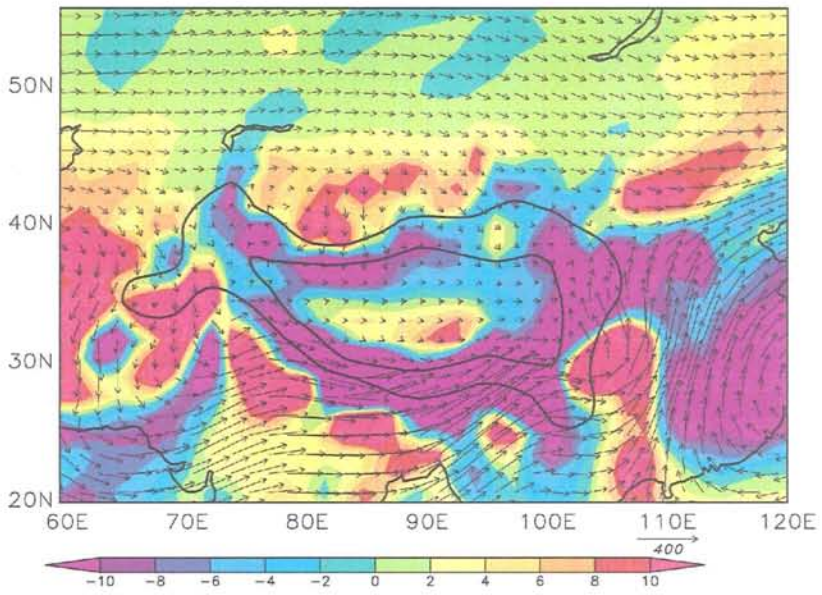

Fig. 3.4: Same with Fig. 3.3 except for LT-NoM run.

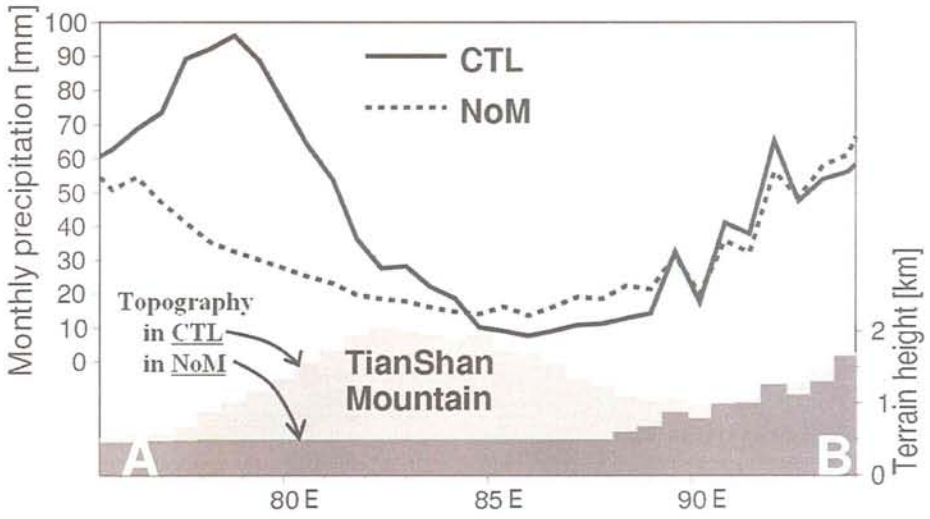

Fig. 3.5: Monthly mean precipitation along A-B line shown in Fig. 3.1. Solid line and dashed line indicate monthly precipitation in LT-CTL and LT-NoM runs, respectively. Light and dark shades in the bottom illustrate the topography in LT-CTL and LT-NoM run, respectively.

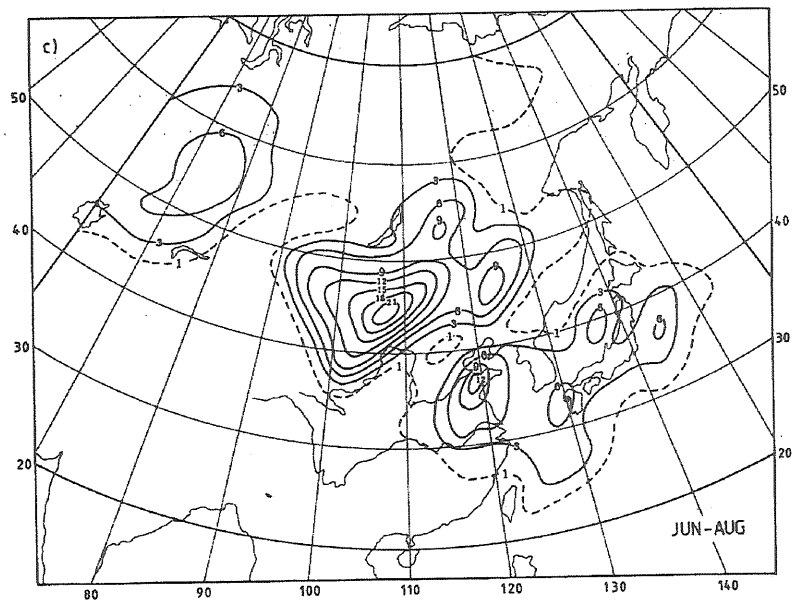

Fig. 3.6: Number of cyclogenesis events (10^{-2}) per 2.5° quadrangle per month in summer for the period 1958-1987. (From Chen et al., 1991)

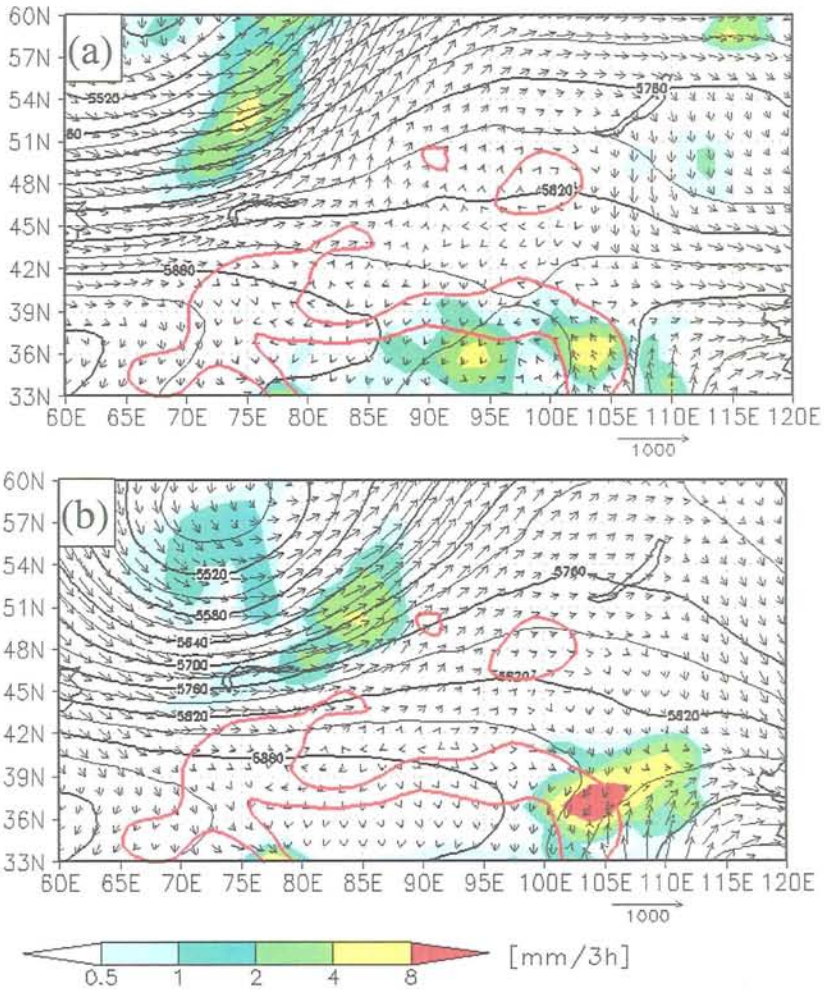

Fig. 3.7: Geopotential height at 500 hPa and vertically integrated water vapor flux (kg m^{-1} sec^{-1}) in LT-CTL run. Three-hourly rainfall is color shaded (mm). Red contours indicate 2000 and 4000 m of the topography. (a) 12 UTC of 17 July 1995, (b) 12 UTC of 18 July 1995.

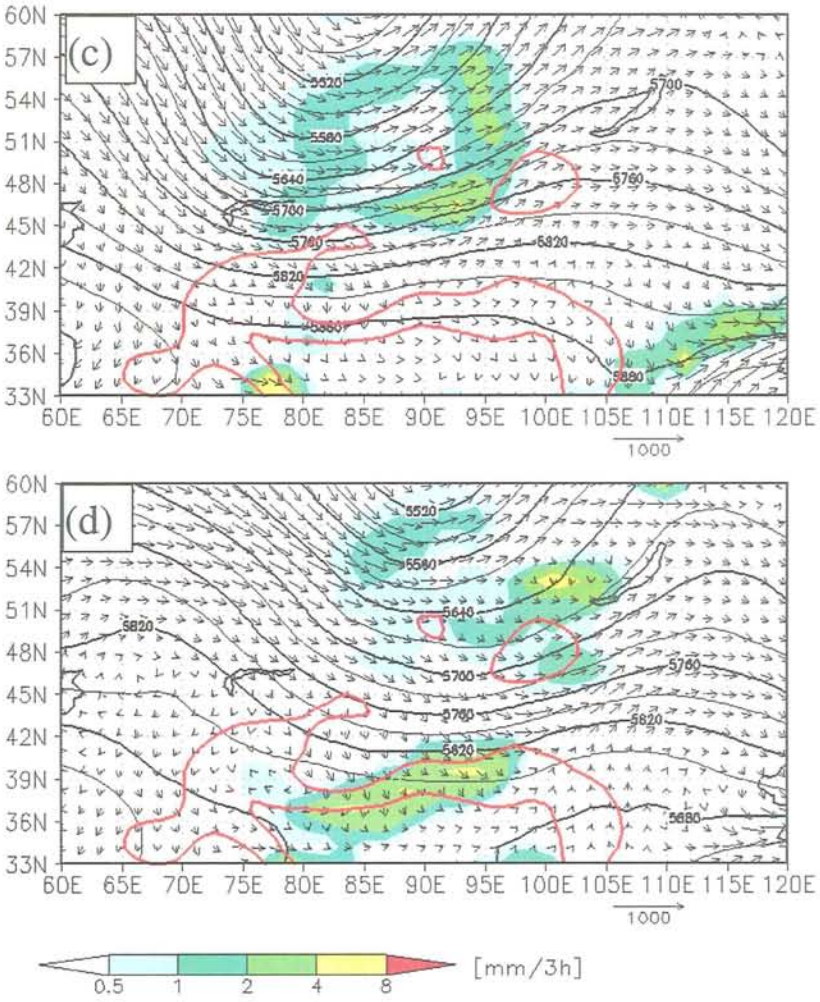

Fig. 3.7: Continued. (c) 12 UTC of 19 July 1995, (d) 12 UTC of 20 July 1995.

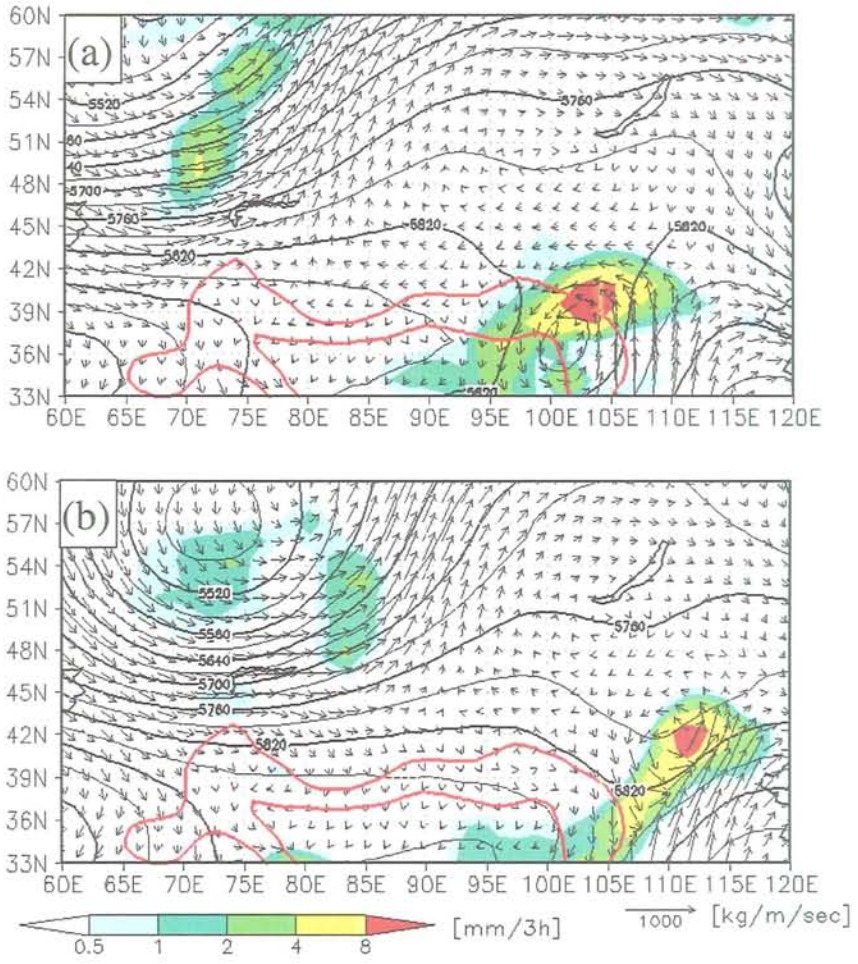

Fig. 3.8: Same with Fig.3.7 but for LT-NoM run. (a) 12 UTC of 17 July 1995, (b) 12 UTC of 18 July 1995.

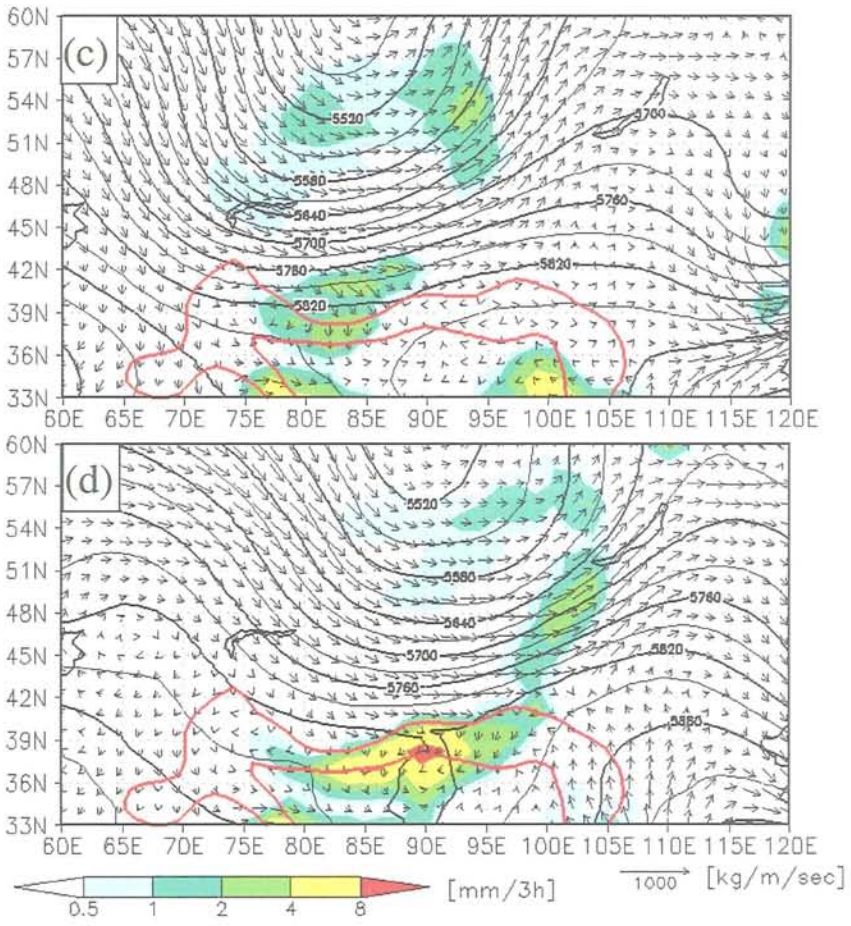

Fig. 3.8: Continued. (c) 12 UTC of 19 July 1995, (d) 12 UTC of 20 July 1995.

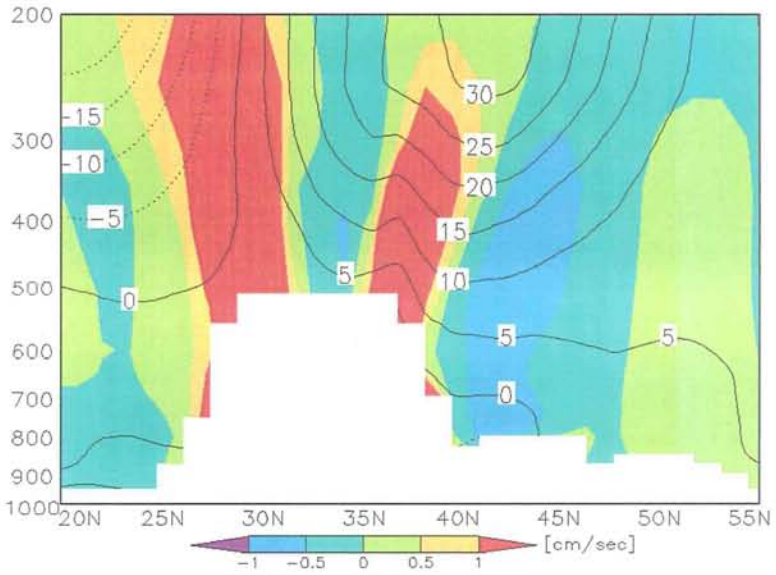

Fig. 3.9: Meridional cross section of ten-year mean vertical motion along 85°E in July by LT-CTL run. Solid contours indicate zonal wind velocity (m sec^{-1}).

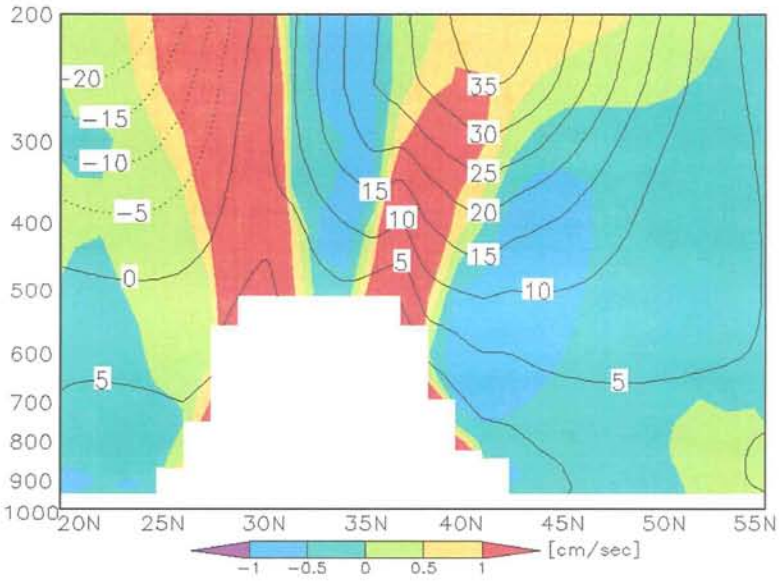

Fig. 3.10: Same with Fig.3.9 but for LT-NoM run.

4. Role of the Tibetan Plateau on the arid climate formation in northeastern Asia

Effect of upwind mountains such as the TianShan Mountains on the formation of the arid climate is found to be negligibly small as shown in the previous section. The both results of LT-CTL and LT-NoM experiments indicate the importance of the prevailing subsidence on the arid climate formation. Motivated by the hypothesis that the subsidence over the arid region decreases the precipitation, further sensitivity experiments are carried out with use of a simple boundary condition. In this section, source of the subsidence is mainly investigated and addressed. Exact settings of each sensitivity experiment described in this section are addressed in Section 2.2, and are briefly listed in Table 2.2.

4.1. Results of zonal mean experiment

Figure 4.1 shows ten-day averaged precipitation and water vapor flux by the ZM-CTL experiment. The features of rainfall distribution are simulated well and aridity in northern China appears even in this experiment around 85°E, 43°N. This indicates that the interaction between zonal mean components and the surface boundary conditions is essential for the formation of the arid area in northern China.

Figure 4.2 illustrates the vertical velocity (shaded) and horizontal wind at the level of 400 hPa. Velocity of the westerly has a maximum around 43°N over East Asia. Distinct descending motion is simulated over Central Asia corresponding to aridity around the Caspian Sea. Another robust downward motion stronger than 1×10^{-2} m sec^{-1} appears on just north of the plateau extending zonally from 81°E to 98°E. In comparison with precipitation of this run (Fig. 4.1), it is apparent that each dry region completely corresponds to the subsidence at this

level. On the other hand, upward velocity is strong around Southeast Asia, the Kunlun Mountain, and Northeast China. These regions are almost equal to the region of heavy rainfall. Figure 4.3 shows vertical cross section in ZM-CTL run. Prevailing subsidence over the arid region is prominent centered on 400 hPa. Diabatic heating in upper troposphere caused by the deep convection induces upward motion over the South Asia.

The vertical motion and horizontal wind at 400 hPa in the ZM-NoC experiment is shown in Fig. 4.4. Ascending motion is not so evident over Southeast and South Asia regions since convection process is turned off in this experiment. However, Fig. 4.4 shows that the steady upward motion is generated over the plateau without condensation process. A robust subsidence motion, greater than 2×10^{-2} m sec^{-1} in magnitude, also appears over the desert region. The level of 400 hPa, shown in Fig. 4.4, corresponds mostly to the mean height of the planetary boundary layer over the plateau. The upward motion should be mainly driven by the sensible heat flux caused by the radiative heating on the plateau surface. Figure 4.5 shows vertical cross section of vertical motion along 85°E. In similarity with Fig. 4.3, downward motion is very strong between 40°E and 50°E showing faster than 2 cm sec^{-1} in middle troposphere. It is very interesting that the upward motion is not so strong over South Asia. In South and Southeast Asia, diabatic heating rate is highest in the world in association with the deep convection. Such feature of the upward motion is absent in ZM-NoC run because the condensation process is turned off in the model so that the diabatic heating by condensation does not occur in middle and upper troposphere. Thus, it means that the heating process inducing the subsidence over the arid region is not always related to condensation heating associated with cumulus convection. Both upward and downward velocities are somewhat strong compared with those of ZM-CTL shown in Fig. 4.2. The difference is mainly caused by too strong downward radiation since cloud formation does not occur in ZM-NoC experiment. In ZM-NoC run, upward motion around the Pamir Plateau and the TianShan Mountain become very strong exceeding 5 m sec^{-1}. The nonlinear interaction between mechanical influence of those mountains and thermal effect of the Tibetan Plateau may exist in ZM-NoC run. However, the author confirmed that the subsidence over the arid region is robustly created when the

TianShan Mountain is removed from ZM-NoC run. Thus, the interaction will be small compared with the thermal effect of the plateau.

Figure 4.6 illustrates the vertical motion and horizontal wind at 400 hPa in the ZM-NoR experiment. Very gentle upward and downward motions are recognized over west and east sides of the plateau, respectively. Nevertheless, amplitudes of the vertical motions are about one tenth of those simulated by the run with radiative heating (Fig. 4.4). Therefore, mechanical influence is expected to be quite small toward the vertical motion during summer, when subtropical westerlies are relatively weak. Additionally, the vertical motion at other levels is very weak in ZM-NoR run (Fig. 4.7). In comparison with Fig. 4.4 and Fig. 4.6, solar radiate heating, instead, plays an important role in the intensification of both upward and downward motion around the plateau. Relationship between the positions of heat source and the downward motion will be discussed in section 4.3.

4.2. Elevated heat source over the Tibetan Plateau

Since the Tibetan Plateau is elevated about 4500 m ASL, its mean planetary boundary layer may extend to middle and upper troposphere. Solar heating on such an elevated surface should widely affect atmospheric circulation (Yanai and Li, 1994). Although quantitive estimation of the diabatic heating is still a difficult issue over such a complex terrain, there are many recent studies which describe the detail nature of heating processes over the Tibetan Plateau (e.g. Ueda et al., 2003; Duan and Wu, 2004).

The results of ZM-NoC and ZM-NoR indicate the importance of diabatic heating, especially radiate heating, to enhance vertical motion around the plateau. In ZM-NoC experiment, solar radiation warms up the ground surface in the whole model domain. This study conducts a ZM-TbQ experiment in which artificial heat source is given on ZM-NoR experiment in order to clarify the region of strong influence on the subsidence. The heat source is placed only over the Tibetan Plateau where ground altitude exceeds 3000 m ASL. Vertical motion and horizontal wind at 400 hPa by ZM-TbQ run is shown in Fig. 4.8. Artificial

heating causes upward motion over the plateau, while downward motion prevails over northern and eastern side of the plateau. Downward velocity is about -0.3×10^{-2} m sec^{-1}. Subsidence in Great Indian Desert is also seen. Horizontal distribution of vertical motion is close to that in the ZM-CTL or ZM-NoC experiment (see also Fig. 4.2, Fig. 4.4). Figure 4.8 indicates that the heating over the plateau does cause the subsidence which reduces precipitation over the desert region. Vertical motion also shows that upward motion prevails corresponding to the artificial diabatic heating over the Tibetan Plateau; as a result, the sinking motion prevails over the arid region, although the amplitude is somewhat weaker. The discrepancy in strength of the subsidence may be caused by the simply assumption of the artificial heat source. Anyway, the diabatic heat over the Tibetan Plateau dose causes the subsidence over the arid region.

Some other sensitivity experiments indicate that the subsidence tends to be stronger when lower layer is heated strongly in case that the total energy of heating is fixed. This indicates that sensible heating associated with daytime mixed layer could be more efficient to enhance the subsidence than condensation heating by cloud physics in upper layer. The results meet with some feature of heating processes over the Tibetan Plateau, for example, Luo and Yanai (1994).

4.3. Response of vertical motion to the heat source

Amount of diabatic heating estimated from reanalysis data is larger in tropical regions, around the Bay of Bengal and Southeast Asia, than that over the Tibetan Plateau (e.g. Rodwell and Hoskins, 1996). Condensation heating contributes large part of the diabatic heating rate in middle and upper troposphere, because convective activity is very high in tropics. Although the relationship between diabatic heating over the Tibetan Plateau and subsidence over the arid region is revealed in section 4.2, diabatic heating process over tropical region may act important role on the subsidence as well. Therefore, ZM-SAQ experiment is attempted by placing the heat source over South Asia instead of the plateau in the same manner with

ZM-TbQ experiment. Figure 4.10 shows ten-day average of vertical motion at 400 hPa during the day 21 to day 30. The figure shows that prevailing subsidence appears only over Central Asia, which is consistent with previous studies. Broccoli and Manabe (1992) showed vertical cross section of the vertical motion simulated by the GCM with and without mountains in globe (Fig. 4.11). They have obtained similar feature of vertical motion with ZM-SAQ experiment. Rodwell and Hoskins (1996) gave an external heating over South Asia in their linearized model indicating a possible relationship between heating over South Asia and descending motion over Central Asia, but not over northeastern Asia (Fig. 4.12). In ZM-SAQ experiment, upward motion prevails over the arid region and around the TianShan Mountain. These results mean that huge amount of diabatic heating over South and Southeast Asia region does not directly affect the subsidence over desert region in northern China.

Rodwell and Hoskins (1996) have suggested that diabatic heating around 25°N is very important to enhance the subsidence over Central Asia, and they found that westward propagating Rossby wave can be simulated if heat source is assumed around equator. However, this study expands the heat source to higher latitude than their study since the Tibetan Plateau will work as an elevated heat source as mentioned in section 4.2. The sensible heat from the Tibetan surface to the atmosphere should be very important because it directly affects middle troposphere where density of the air is low, even though total heating rate is smaller than that in tropical regions.

In this study, the diabatic heating over the plateau seems to initiate Rossby wave and gravity wave, which can propagate northern side of the heated region because subtropical jet runs higher latitude, and then forms almost stationary states. Although response to the heat source is somewhat disturbed by orographic perturbation, vertical motion looks very similar to that shown by Rodwell and Hoskins (1996). In north of the Tibetan Plateau, zonal mean westerly modifies the stationary wave causing the subsidence to northwest of the heat source. Figure 4.13 illustrates the schematic diagram showing the formation mechanism of subsidence over the arid region. Diabatic processes, such as solar radiation and cloud condensation, heat up the atmosphere over the Tibetan Plateau. The diabatic heating causes stationary wave

inducing subsidence over the arid region by interaction with mid-latitude westerly, since subtropical westerly jet in upper troposphere runs north of the plateau during summer. Further investigation on the relationship between stationary subsidence and zonal mean flow is discussed by idealized experiment in section 5.1.

4.4. Summary

The reason of robust descending motion over the arid region in northeastern Asia, which reduces the precipitation, is investigated by sensitivity experiments using regional climate model. The descending motion tends to be very weak when diabatic process is turned off in the model in ZM-NoR experiment. On the other hand, radiation process strongly enhances the subsidence over the arid area even though the condensation heating is absent in the model.

Diabatic heating over the Tibetan Plateau leads to a generation of Rossby wave. The stationary wave tends to propagate northward because subtropical westerly jet is being situated north of the plateau in boreal summer. Therefore, the stationary descending motion prevails over northeastern Asia, which consequently reduces the precipitation around arid region. Diabatic heating over tropical region does not affect directly over the desert since the position of subtropical westerly is not favorable to cause the subsidence in the arid region.

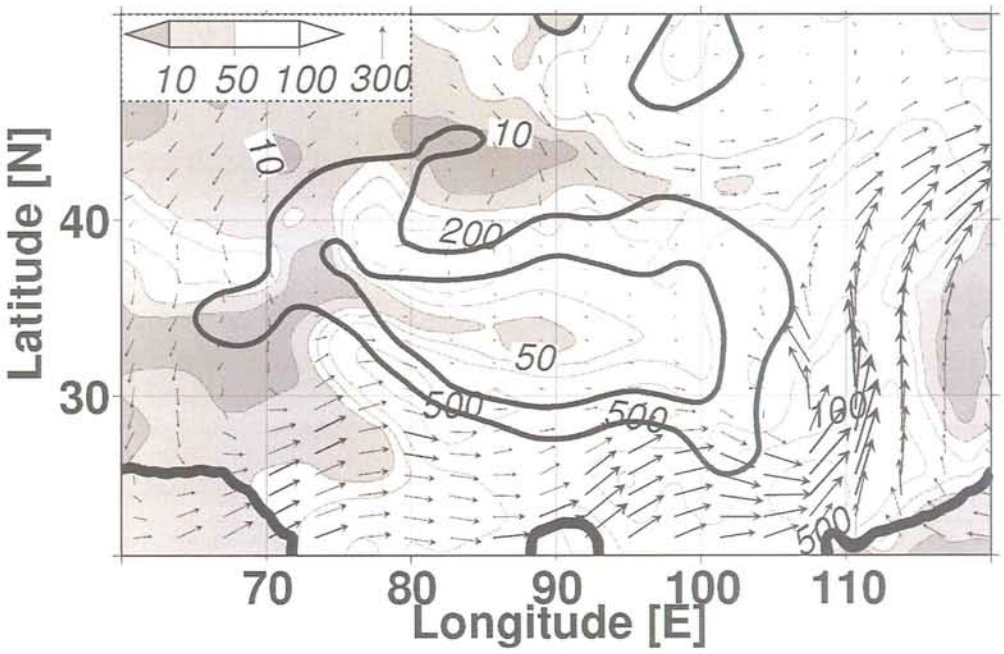

Fig. 4.1: Simulated mean precipitation (mm month^{-1}) and water vapor flux (kg m^{-1} sec^{-1}) in ZM-CTL experiment. Thick solid contours indicate 2000 and 4000 m of the topography.

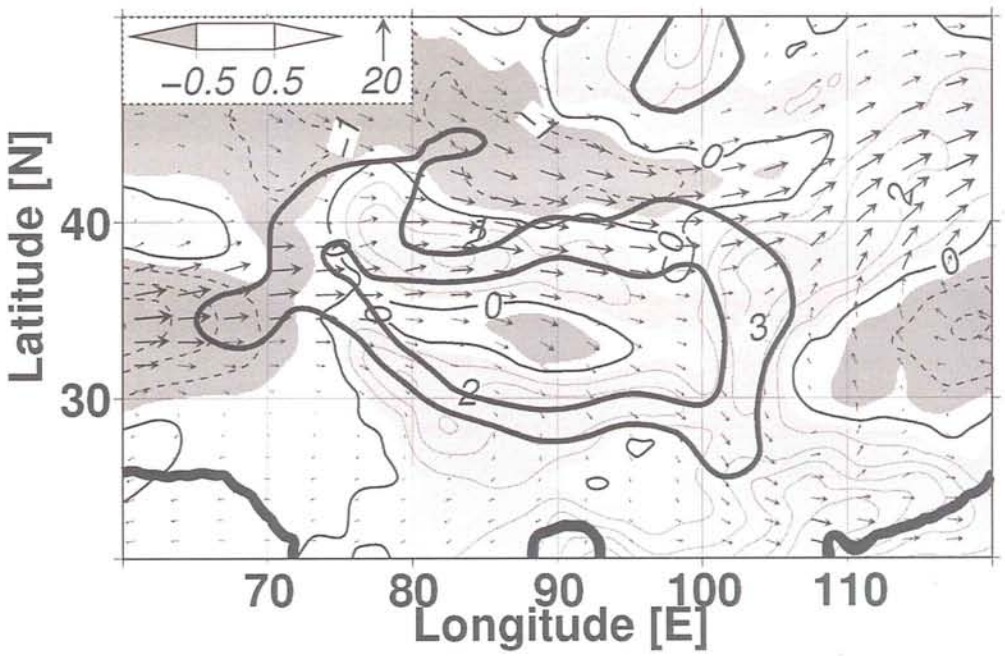

Fig. 4.2: Mean Vertical velocity (cm sec^{-1}: shaded) and horizontal wind speed (m sec^{-1}) at 400 hPa in ZM-CTL experiment. Solid contours and light-shaded regions indicate positive (upward) vertical velocity in each 1 cm sec^{-1}, while dashed contours and dark-shaded regions indicate negative (downward) velocity. Thick solid contours indicate 2000 and 4000 m of the topography.

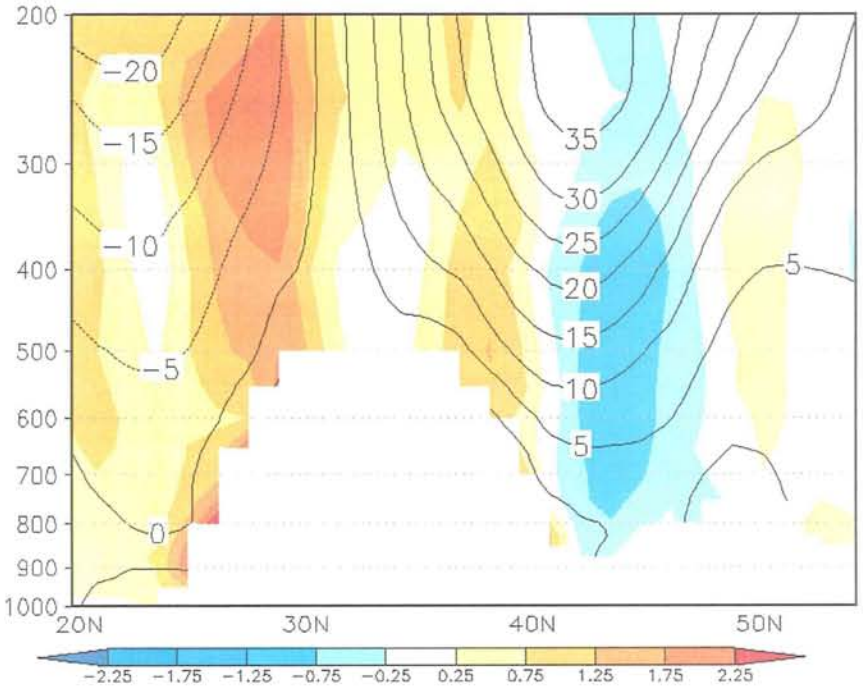

Fig. 4.3: Meridional cross section of vertical motion along 85°E by ZM-CTL run (cm sec^{-1}). Solid contours indicate zonal wind velocity (m sec^{-1}).

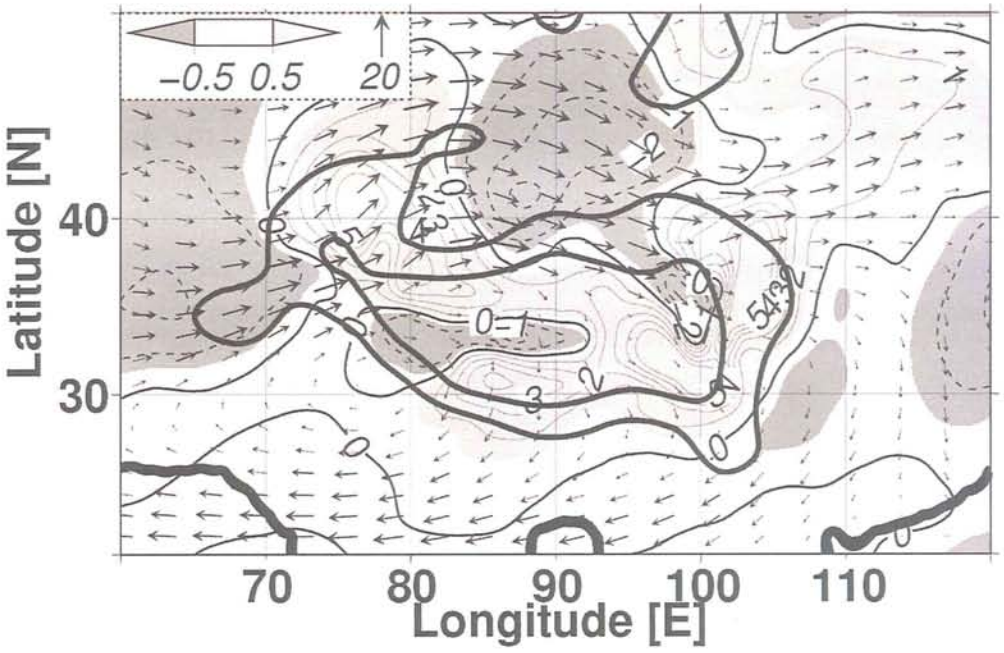

Fig. 4.4: Same with Fig. 4.2 but for ZM-NoC run.

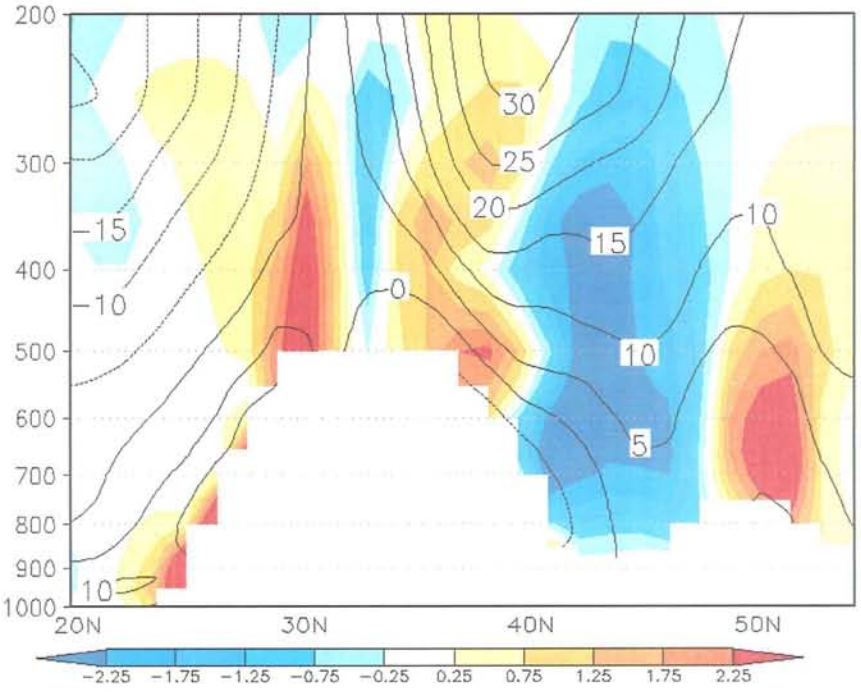

Fig. 4.5: Same with Fig.4.3 but for ZM-NoC run.

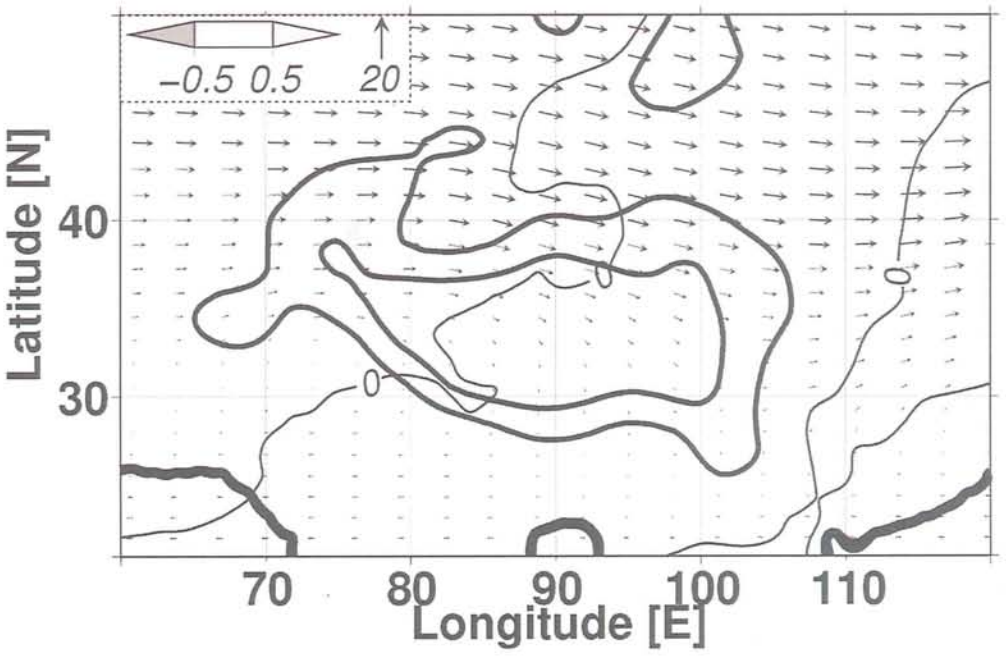

Fig. 4.6: Same with Fig. 4.2 but for ZM-NoR run.

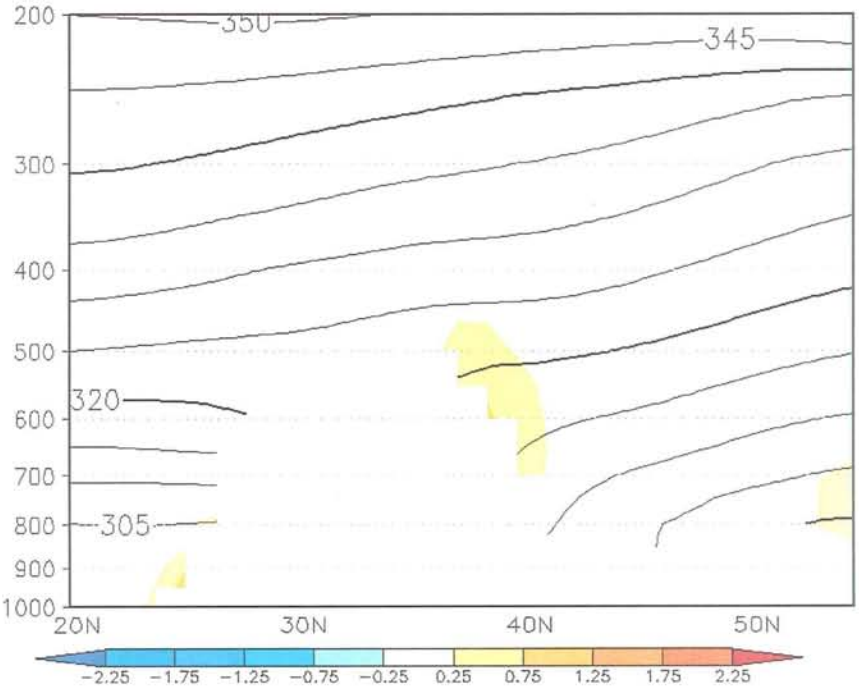

Fig. 4.7: Meridional cross section of vertical motion along 90°E by ZM-NoR run (cm sec^{-1}). Solid contours indicate potential temperature (K).

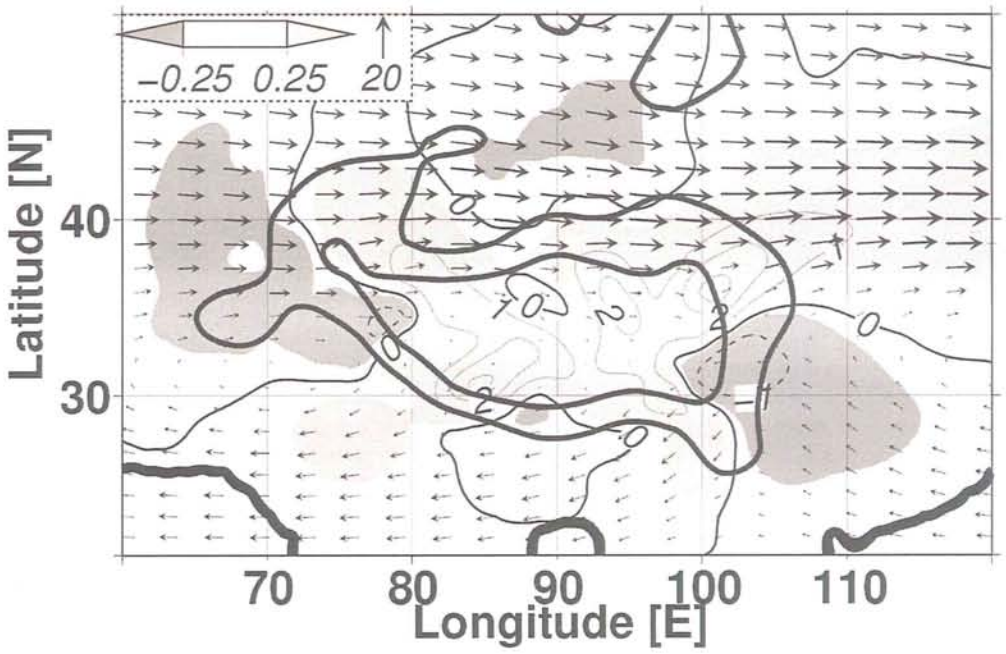

Fig. 4.8: Same with Fig. 4.2 but for ZM-TbQ run.

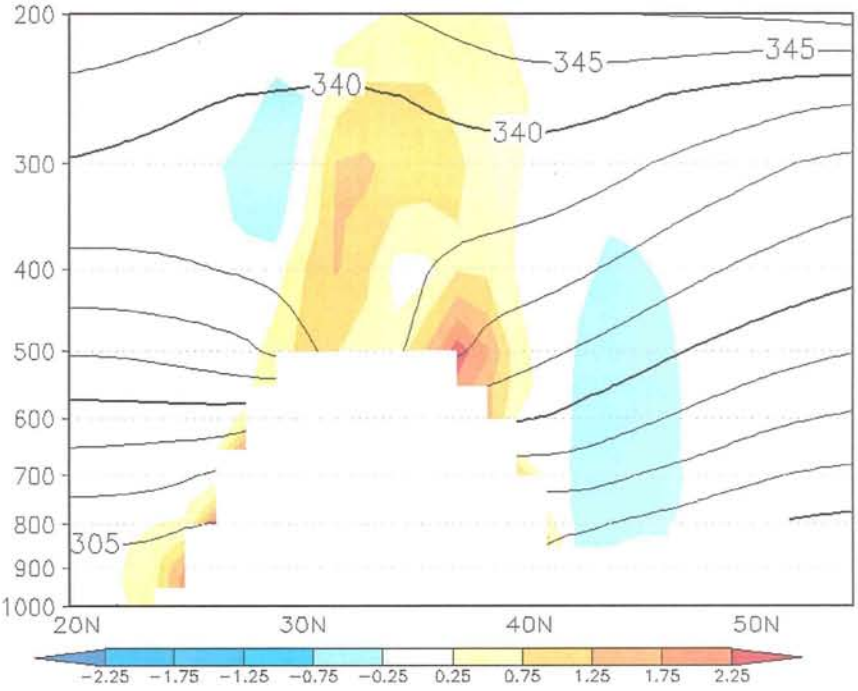

Fig. 4.9: Same with Fig.4.7 but for ZM-TbQ run.

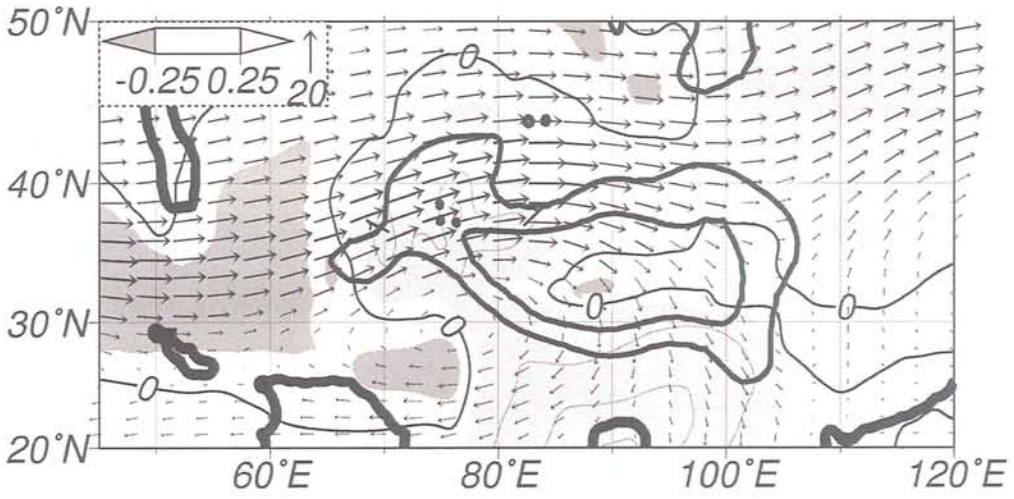

Fig. 4.10: Same with Fig. 4.2 but for ZM-SAQ run.

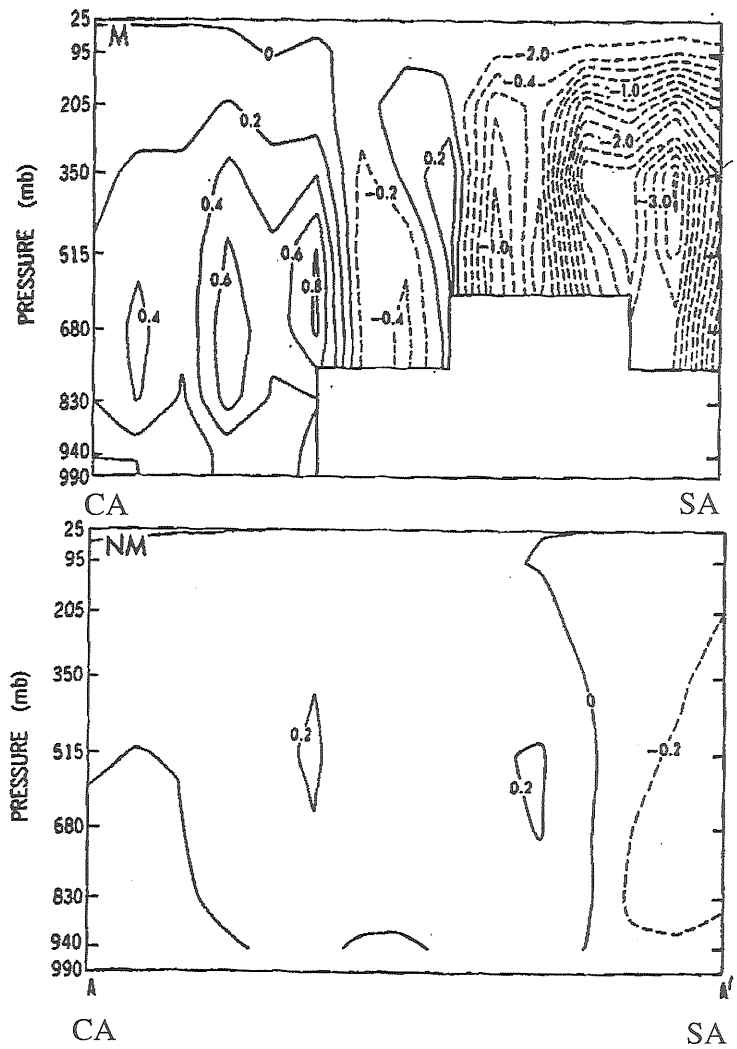

Fig. 4.11: Cross section of vertical p-velocity (dyn cm^{-2} sec^{-1}) between Southeast Asia (SA) and Central Asia (CA) simulated by GCM with mountain (upper) and without mountain (lower). (After Broccoli and Manabe, 1992)

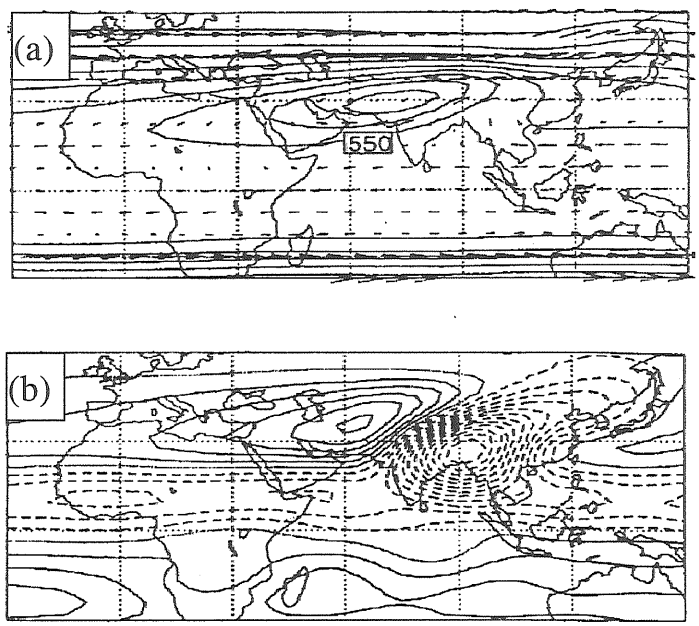

Fig. 4.12: (a) Pressure and horizontal winds on the 325 K isentropic surface, with contour interval 40 hPa simulated by linearized model. (b) Vertical velocity at 477 hPa, with contour interval 0.25 hPa hr^{-1}. (From Rodwell and Hoskins, 1996)

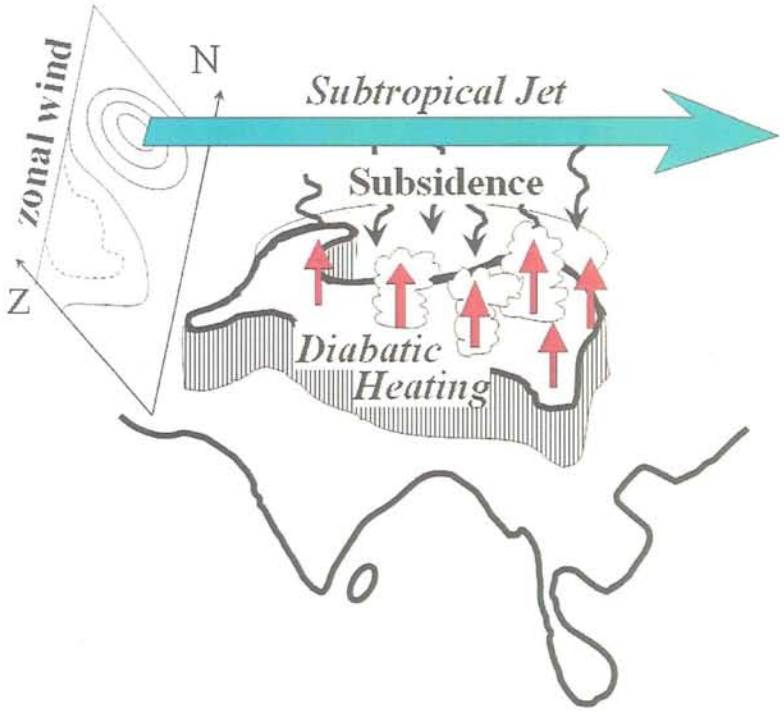

Fig. 4.13: Schematic diagram showing the formation of subsidence over arid region in northeastern Asia.

5. Discussion

5.1. Connection to the seasonal evolution in East Asia

Figure 5.1 shows the global zonal mean of zonal wind velocity at 200 hPa in 1998. In general, subtropical westerly jet in upper troposphere retreats poleward during summer. It runs completely north of the Tibetan plateau, approximately 30°N to 40°N during June to September when diabatic heating over the plateau becomes much stronger. Similar features of seasonal variation are seen in middle troposphere (500 hPa) as shown in Fig. 5.2. Westerly jet exists around 30°N in boreal winter, while it prevails around 45°N during June to September. In lower latitude, easterly wind prevails during boreal summer.

As mentioned by Hoskins (1996), the mid-latitude subsidence is likely to be accelerated according to the interaction between Rossby mode and subtropical westerly jet. In current study, ZM-AQUA experiments are carried out in which topography is assumed to be flat; and surface is covered by the ocean like aqua planet experiment. The Tibetan-plateau-shaped column heat source is added on the same location with ZM-TbQ experiment. Zonal mean fields for each month are calculated from NCEP/NCAR reanalysis to use as a boundary condition of numerical experiments. Ten-day average is computed during 21 and 30 days after the integration to evaluate the steady state of atmospheric response to the heat source. Figure 5.3 illustrates the vertical motion at 500 hPa for each month simulated by ZM-AQUA experiments. Coastlines drawn by dashed lines in the figure are dummy to identify the geographical location since whole numerical domain is covered by the ocean in this run. During January to March, robust subsidence, greater than 2 cm sec^{-1}, is formed in south and southwest of the Tibetan-plateau-shaped heat source as well as weak subsidence over north of the heated region. Since westerly wind tends to prevail around 30°N in this season, ten-day average zonal wind shows maximum around the south of heated region (Fig. 5.3b, c, d). But westerly is still strong around 40°N, which makes another peak of zonal wind velocity in the

north of heated region around 40°N. In April, horizontal distribution of vertical motion exhibits meridionally symmetric structure toward the plateau-shaped heat source (Fig. 5.3e). During June through September, westerly wind in the middle troposphere becomes very weak in lower latitude zone as shown in Fig. 5.2. Stationary states of the zonal wind for these months (Fig. 5.3g, h, i, j) also indicate the similar pattern with real atmosphere in respect with zonal wind. Vertical motion for these months shows very different with the winter season as mentioned above. The subsidence prevails to the west and north of the heat source in June. Almost the same distributions with ZM-TbQ experiment (Fig. 4.8) are obtained in July and August, which is consistent that diabatic heating over the plateau will cause subsidence over northern China during summer. Relationship between the heated region and subsidence is very clear in ZM-AQUA run since any mountains and any land-sea contrasts are absent. The subsidence tends to prevail in the south of the heat source as well as to the north in October and November synchronized that subtropical westerly moves to southward.

As summarized by Wang and LinHo (2002), onset date of the summer Indian monsoon varies depending on the region (Fig. 5.4). In northeastern India, the onset of monsoon rainfall occurs in early June, while it occurs in middle July in northwestern India. The prevailing subsidence in ZM-AQUA over India disappears through May to July (Fig. 5.3f, g, h), which agrees very much with the observed seasonal variation of onset date, despite very simple assumptions are made in the experiment. Additionally, the appearance of prevailing subsidence occurs during September and October in ZM-AQUA (Fig. 5.3j, k), which is consistent with the withdrawal date of the Indian summer monsoon (Fig. 5.4). Hence, this paper suggests that the onset of summer Indian monsoon can be strongly affected by the relationship between diabatic heating over the plateau and subtropical westerly. The stationary subsidence in middle troposphere should suppress convective activity even over tropical regions.

Figure 5.5 and Fig. 5.6 illustrate latitude-time diagram of the ten-day averaged vertical motion at 500 hPa along 80°E to 90°E in ZM-AQUA and ZM-FLQ experiment, respectively. Temporal and Spatial patterns of two experiments show almost same feature with

respect to the subsidence as addressed above; thus, land-sea contrast does not so important to modify the effect of diabatic heating in ZM-FLQ. In comparison to Fig. 5.2, zonal wind velocity shows similar seasonal variation with real global mean zonal velocity. It is very important to note that the subsidence around the heat source is in good agreement with the latitudinal position of westerly jet for each month. This means that the descending motion may prevail even in winter in vicinity of the plateau. Although the focus of this study is in Northeast Asia, thermal effect of the Tibetan Plateau may reach over South and Southeast Asia in case that subtropical jet extends to south of the Tibetan Plateau. Role of zonal wind to determine the region of subsidence would be considered as follows. The artificial heat source causes a generation of gravity wave and westward propagating Rossby wave. Velocity of subtropical jet in upper troposphere would be equal or stronger than propagating speed of the Rossby wave; then, Rossby wave can be stationary causing subsidence corresponding to the velocity of subtropical westerly as well as to immediate west of the heat source. Similarly, subsidence often appears over southwest of the heated region around 75°E, 30°N due to characteristic shape of the heat source, namely, shape of the Tibetan Plateau. Additionally, perpendicular component of the wind to the artificial heat boundary would be also important to form subsidence around the heated region. Since the heated region persists high potential temperature, air flow blowing toward the heated region can be regarded as relatively cold wind. Assuming the isothermal flow, cold wind causes the subsidence near the boundary of heated region where gradient of isothermal surface exists.

Figure 5.7 and Fig. 5.8 shows seasonal variation of zonal wind velocity averaged around the Tibetan Plateau, between 80°E and 90°E. Regardless to say, zonal mean for the particular region is often different from the global zonal mean. For East Asia, the Tibetan Plateau and surrounding mountainous region is a physical barrier for zonal flow. The subtropical jet locates completely south of the Tibetan Plateau during boreal winter. And poleward retreat of the subtropical jet occurs more suddenly around May to June than it can be seen in global zonal mean, which should make the appearance of the subsidence more drastic over the arid region.

5.2. Consistency of simulated behavior with the observed evidence

Summer precipitation based on surface observation tends to show an opposite phase between northeastern and southeastern Tibetan Plateau (e.g. Liu and Yin, 2001). Yatagai and Yasunari (1994) also revealed a similar distribution of summer precipitation. Their statistical results indicate that there is a negative correlation in precipitation between northeastern China and eastern Tibetan Plateau (Fig. 5.9), although unfortunately stations are not enough over the Tibetan Plateau. The typical pattern can be explained as follows. More frequent convective activities in eastern Tibetan Plateau causes large amount of diabatic heat as a result of condensation. As shown in ZM-CTL experiment, diabatic heating in this region will enhance the subsidence over desert area, thus, precipitation is likely to be suppressed. In opposite, if diabatic heating rate is small due to less active convection, subsidence over the arid region tends to be weak that may allow precipitation to occur over the arid region in relation to the synoptic scale disturbances.

Yanai and Li (1994) summarized upper sounding data to estimate the distribution of vertical velocity over and around the Tibetan Plateau (Fig. 5.10). Their results in vertical motion for 4-months mean are reliable since it was computed in a basis of in-situ upper air soundings. They found that vertical motion above most part of the plateau is upward, while descending motion prevails corresponding to the desert region, which is very similar to that in ZM-TbQ run (Fig. 4.8). Upward motion is not distributed uniformly over the plateau, and some typical downward features are recognized over north, southwest, and southeast of the Tibetan Plateau. The subsidence appeared over north and southwest of the plateau is well corresponding to the desert climate. All of these three prevailing downward motions are recognized in ZM-TbQ run. Thus, it can be considered that the observed vertical motion is mainly caused by the diabatic heating over the Tibetan Plateau. Additionally, Yanai and Li (1994) suggested that there is a distinct diurnal variation in vertical velocity around the Tibetan Plateau. This could be also the reason that sensible heat flux from the plateau surface plays an important role to drive the subsidence over the arid region. Recent accumulation of

the observational and analytical efforts have gradually improved the understanding on detail nature of diabatic heating and convective activity over the Tibetan Plateau including vertical structure, horizontal distribution, and temporal variation. Most part of their findings will be deeply related to the desert climate variation altering convective activity over the desert through the variation of the subsidence.

5.3. Role of local mountains on cloud formation

In northeastern Asia, the number of cyclogenetic events is very high around central Mongolia whole the year in relation with the Altai-Sayan lee cyclogenesis (Chen et al., 1991). As described in Section 3.1, it is suggested that these mountain ranges are very important to cause precipitation in the lee of them. Difference of precipitation regime between LT-CTL and LT-NoM indicates that the complex terrain in central and western Mongolia greatly contributes to precipitation around the arid region rather than decrease rainfall as a barrier of water vapor transport. The roles of mountains on precipitation and cloud systems enhancement in study area are described in this section.

Sato et al. (2004) have investigated cloud frequency over Mongolia and northern China by composite analysis of Geostationary Meteorological Satellite (GMS) visible channel data in August during 1998 to 2001. Figure 5.11 illustrates detail topography and geographical names in analyzed domain. As it is evident, very complex terrain covers northern China and Mongolian territory. Twenty-years average NDVI (Normalized Difference Vegetation Index) in middle August is shown in Fig. 5.12. The original NDVI data is distributed as the Normalized Difference Vegetation Index (NDVI) Twenty-year Global 4-minute AVHRR NDVI Dataset by CEReS (Center for environmental Remote Sensing, Chiba University). Compared with land surface characterization (Fig. 1.3), NDVI is very low with less than 0.1 near border between China and Mongolia, and gradually increasing to forest in northern Mongolia. Additionally, the NDVI is relatively high over the mountain commonly even over the arid region.

Figure 5.13 shows composite of cloud frequency in August over eastern Mongolia. In 08 LT (Local Time), most part of analyzed domain shows less than 10 % except for the northern part of Mongolia and around the Lake of Baikal. High frequency is found over southeastern region of the domain, eastern edge of the Altai Mountains, and the Khentei Mountain with 20 to 30 %. High frequency regions at 08 LT continuously keep high values in 10 LT; especially it exceeds 35 % near top of the Khentei Mountain (Fig. 5.13b). The frequency increases close to 30 % over east of the Khangai Mountain. Highest region of cloud frequency is located in northwest of the Khentei Mountain over Russia. At 12 LT, the frequency retains 40 % in many grids over the Khentei Mountain, which means that this region is covered by cloud around noon in 12 days in August (Fig. 5.13c). Over grassland, the frequency gradually increases up to 30 % in maximum at 14 LT (Fig. 5.13d). However, the frequency is low in relatively low altitude grassland around 115°E, 47°N or semi-basin region surrounded by the mountain, e.g. 104°E, 45°N and 103°E, 49°N. In northern China around 107°E, 41°N, cloud frequency is low over vegetated surface; on the other hand, relatively high frequency is found over less- or non-vegetated mountain in vicinity. In 16 LT, cloud frequency reaches its maximum in diurnal cycle in all over the analyzed domain (Fig. 5.13e). The highest regions distribute around the Khentei Mountain, the Khangai Mountain, and the Sayan Mountain exceeding 50 % in maximum. The lowest frequency appears near the Taklimakan desert and the Lake of Dallay and the Lake of Baikal.

Land surface condition of Mongolia can be roughly classified in desert, grassland, and forest regions. In general, evapotranspiration plays an important role on the precipitation in global scale (Shukla and Mintz, 1982). However, as it is shown in Fig. 5.13e, cloud is likely to be observed over mountainous region, and is hardly observed over lake or humid land covers. Over vegetated or water surfaces, the latent heat flux tends to be larger due to the larger evapotranspiration than that over desert or sparse grassland. Sensible heat flux over such condition becomes relatively small due to the radiative energy partitioning. Therefore, the humid surface hardly causes the cloud formation, although the water vapor is abundant due to relatively large evapotranspiration. These results do not conflict with previous sensitivity

study by Lee and Kimura (2001). Grassland or forest vegetation prevails over the mountain; thus, vegetation circulation may occur due to the horizontal contrast of sensible heat flux between mountain and surrounding regions. However, the contrast does not seem enough to drive the vegetation circulation against anabatic circulation.

The mountain efficiently accumulates the water vapor as a result of mountain circulation in clear daytime (Sato and Kimura, 2005). Additionally, the mountain slopes often act as a barrier of an environmental flow, causing a forced lifting of the air mass. Therefore, cloud frequency is higher in eastern edge of the Altai Mountain, where relatively dry climate near desert, than semi-basin area in north of the mountain. The frequency is lower in mountain foot around 104°E, 49°N in the Khangai Mountain despite that evapotranspiration should be larger due to the existence of forest and grassland. By these reasons, the appearance of the cloud over Mongolia is less sensitive to surface condition than that induced by terrain slope.

Difference of maximum frequency between the Khentei Mountain and the Khangai Mountain is evident, even though the altitude and the width of the mountain are considered to be almost same. It would be caused by the topography around the mountain. The Khentei Mountain has a large open area in upwind against the prevailing synoptic-scale northwesterly wind. Precipitable water vapor in upwind of the Khentei Mountain is much larger than that in upwind of the Khangai Mountain, because it is strongly dependent on ground altitude. Such differences maintain the more favorable condition for cloud formation over the Khentei Mountain. In general, inhomogeneity of surface properties affects the atmospheric circulation and cloud formation. By this analysis using GMS data, it is obvious that water surface of lakes largely affects the modification of cloud frequency. But the modification is not to enhance but to decrease the cloud formation in contrast. Therefore, the influence of topography to cloud formation is much larger than that induced by vegetation contrast.

Before long, the mountain range such as the TianShan, the Altai and the Sayan Mountains are believed to decrease precipitation in its lee side owing to the rain-shadow effect. By this study, actually, the mountain ranges are not the reason of the arid climate, but they are very important to generate cloud and cyclogenesis in its lee side. Prominent meridional

gradient of annual and summertime precipitation in northeastern Asia, between the Gobi desert and Taiga in Siberia, is strongly emphasized by two reasons. The first one is rainfall suppression by the subsidence in desert region as described in section 4. The second reason is deemed with the topographical contrast between relatively flat topography in desert regions and complex terrain in northern and northwestern Mongolia. As mentioned in this section and section 3, rainfall tends to occur around northern mountainous region and lee of the mountains due to mechanical and thermal effect of the mountain. The combination of these two causes maintains the characteristic difference in precipitation between desert and surrounding areas.

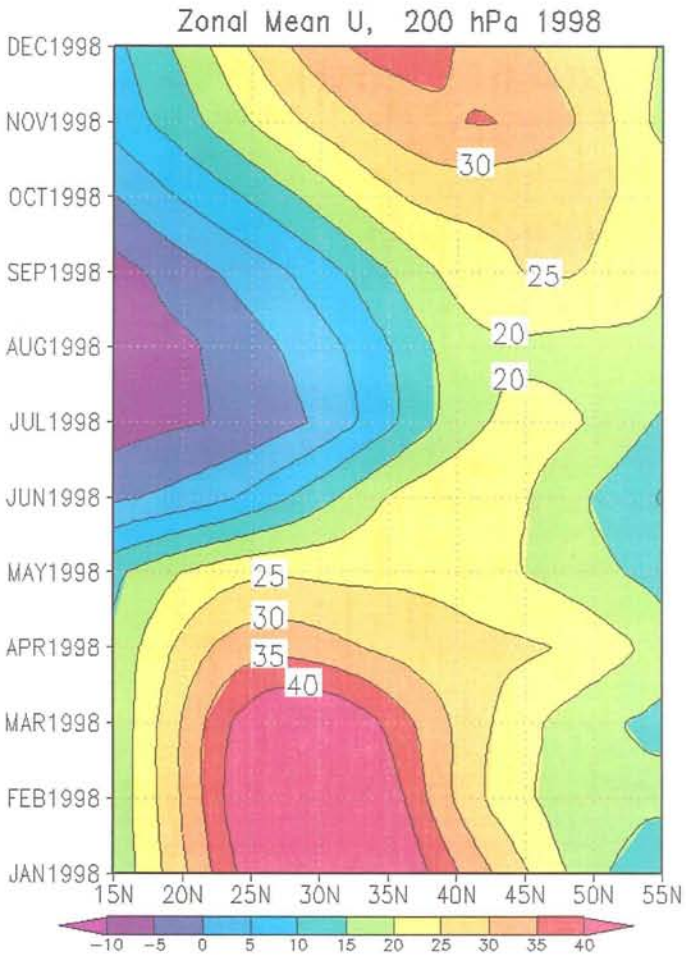

Fig. 5.1: Seasonal variation of global zonal-mean zonal wind (m sec^{-1}) at 200 hPa in 1998.

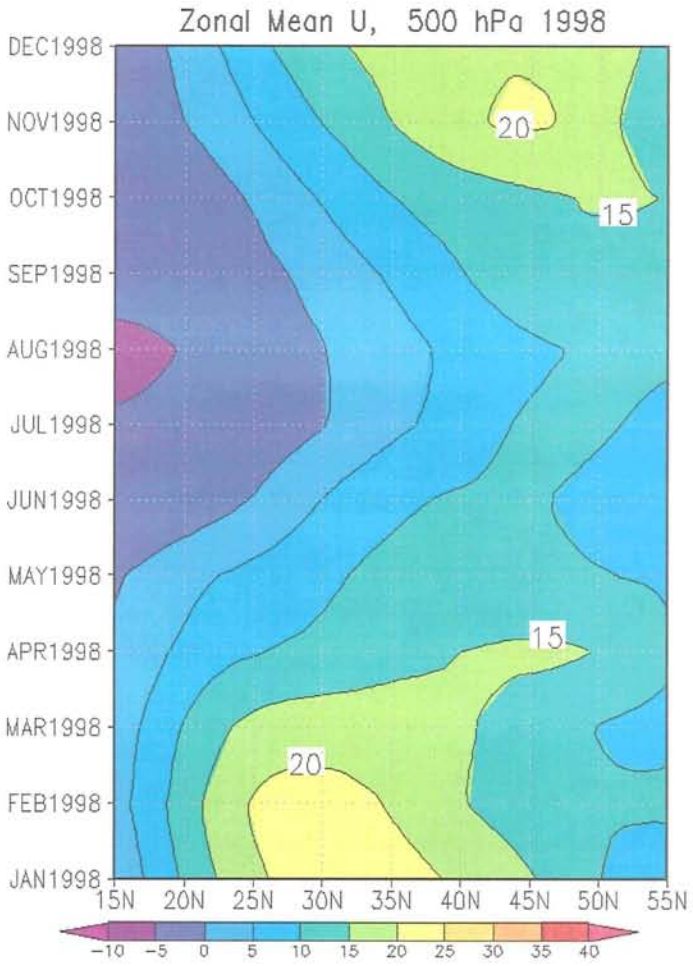

Fig. 5.2: Same as Fig. 5.1 but for 500 hPa.

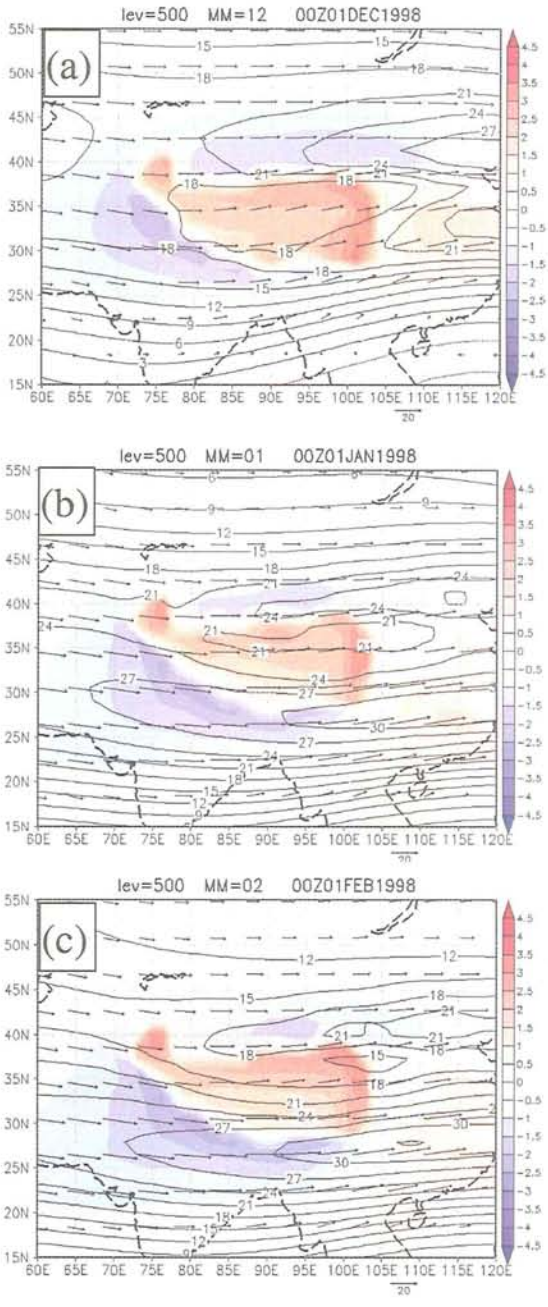

Fig. 5.3: Ten-day averaged vertical wind velocity (cm sec^{-1}: shaded), zonal wind velocity (m sec^{-1}: contour), and wind vectors at 500 hPa in ZM-AQUA experiment. Coastlines are drawn as dummy because of aqua planet experiment. (a) December, (b) January, (c) February.

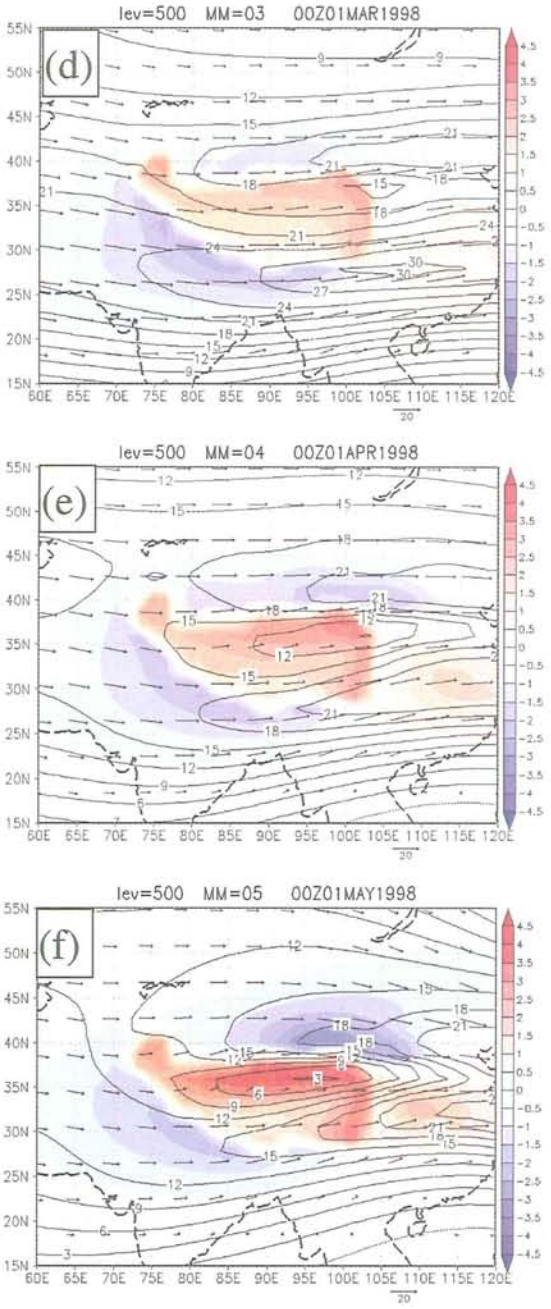

Fig. 5.3: Continued. (d) March, (e) April, (f) May.

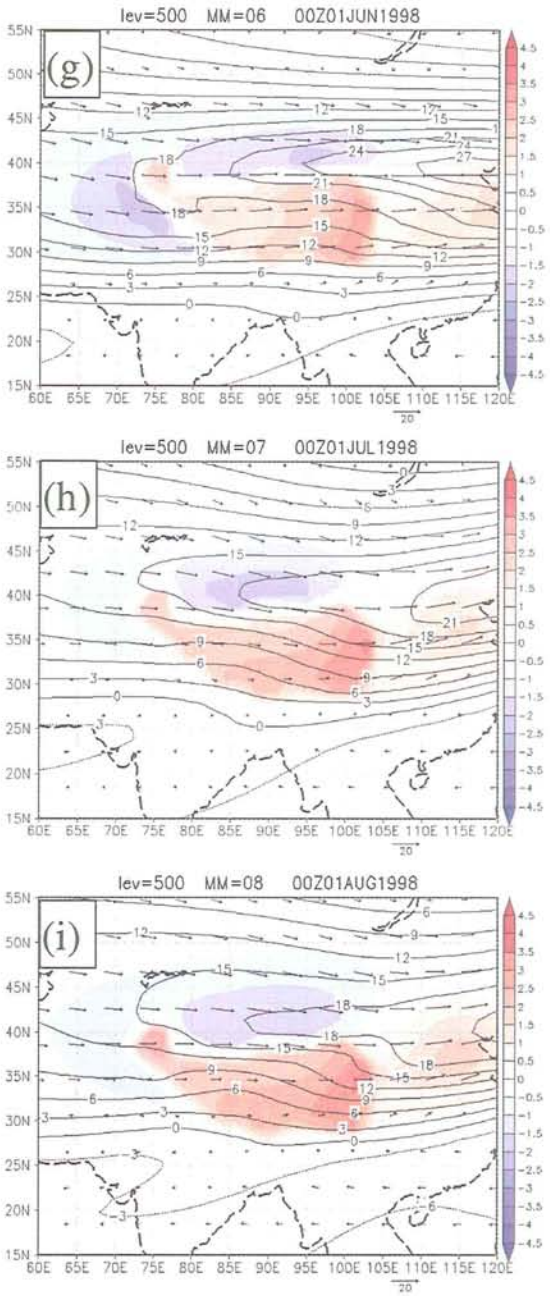

Fig. 5.3: Continued. (g) June, (h) July, (i) August.

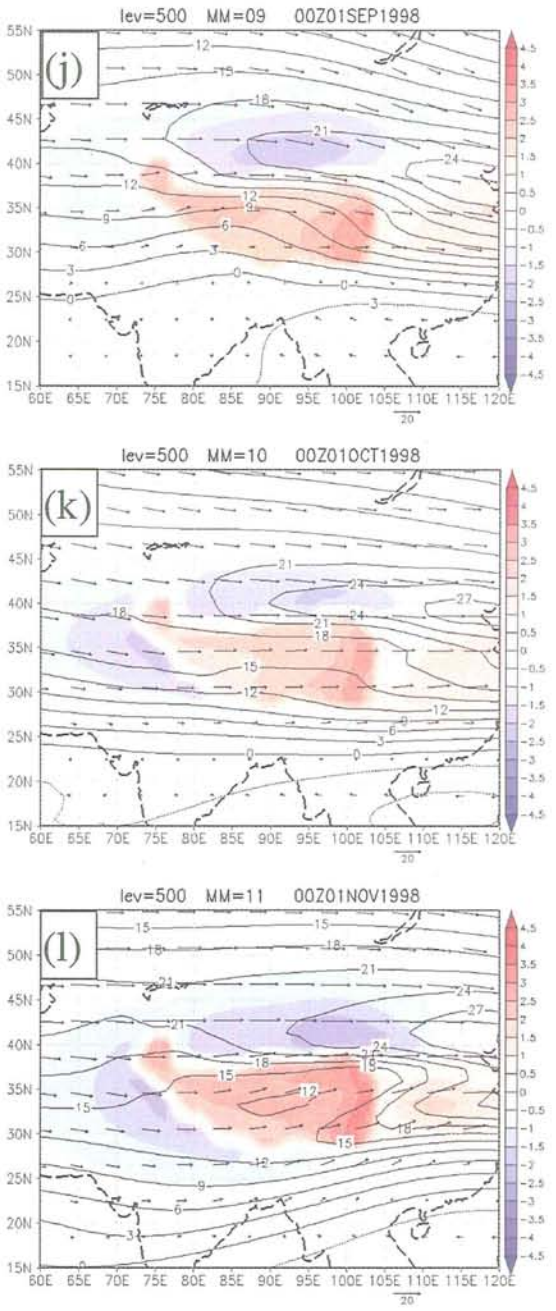

Fig. 5.3: Continued. (j) September, (k) October, (l) November.

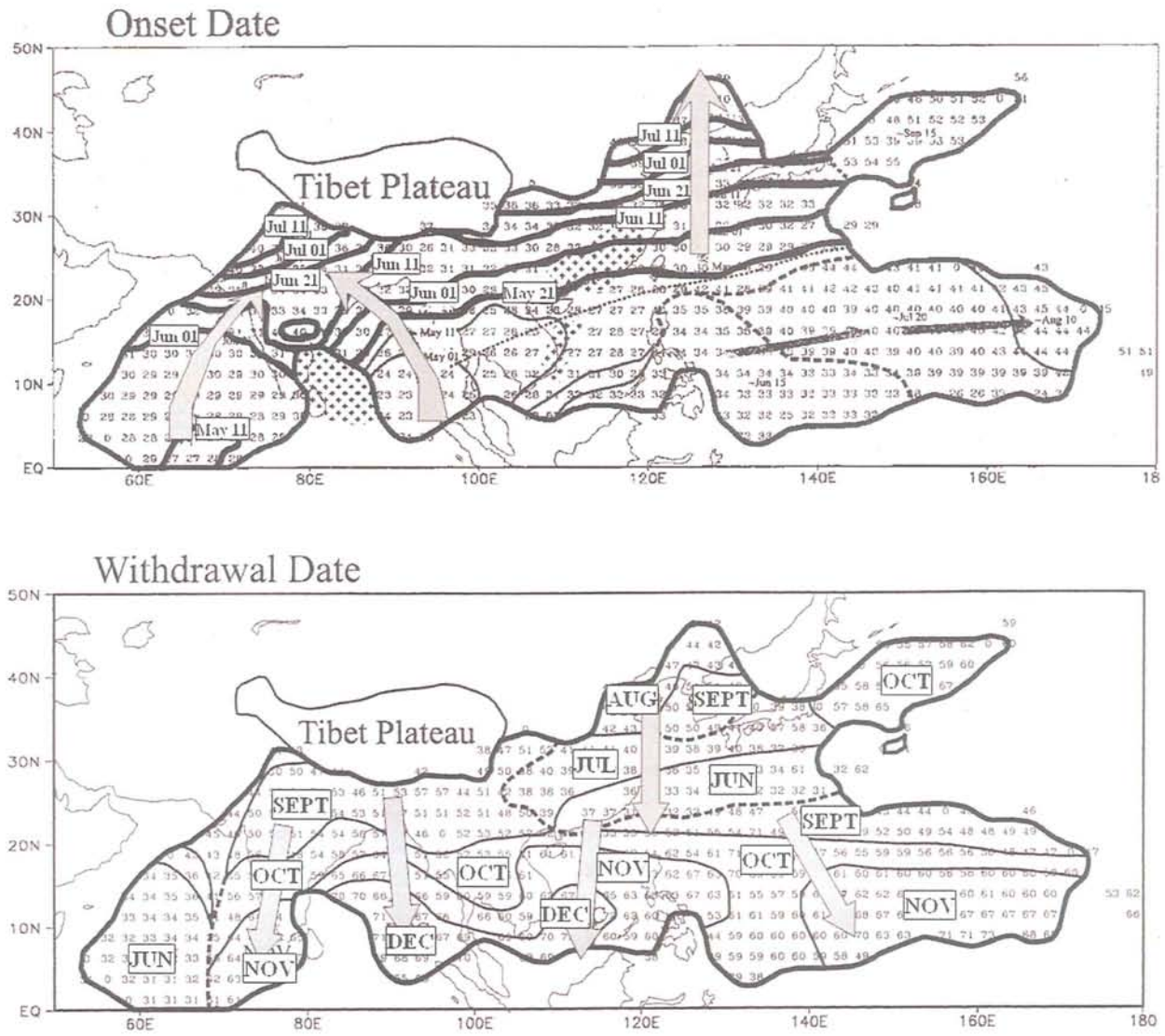

Fig. 5.4: Dates of onset (upper) and withdrawal (lower) of summer monsoon determined by climatological pentad mean rainfall data. (After Wang and LinHo, 2002).

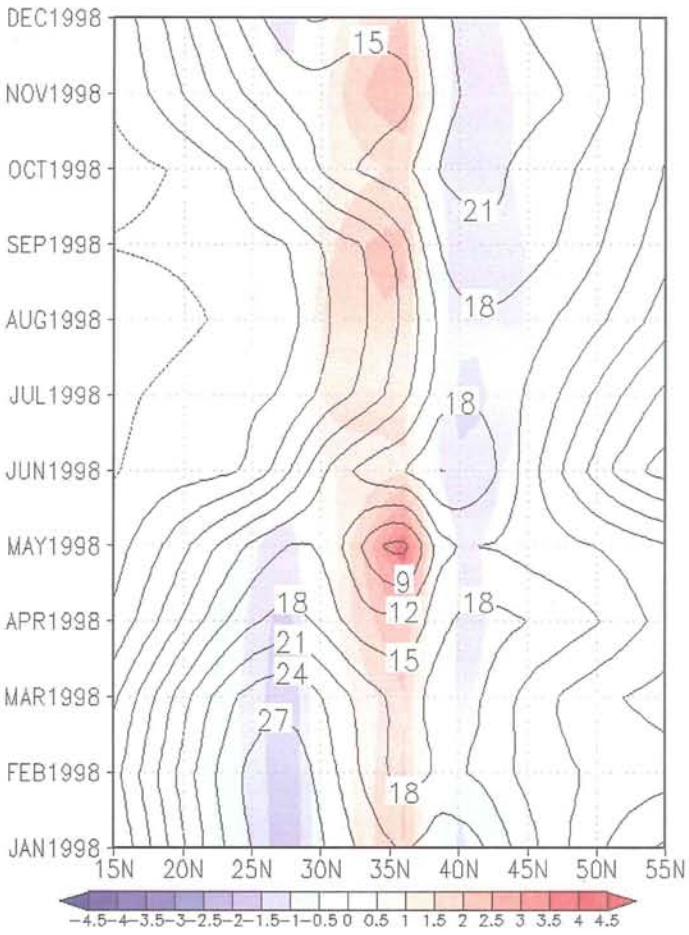

Fig. 5.5: Seasonal variation of vertical velocity (cm sec^{-1}: shaded) and zonal wind velocity (m sec^{-1}: contour) at 500 hPa averaged between 80°E and 90°E in ZM-AQUA experiment.

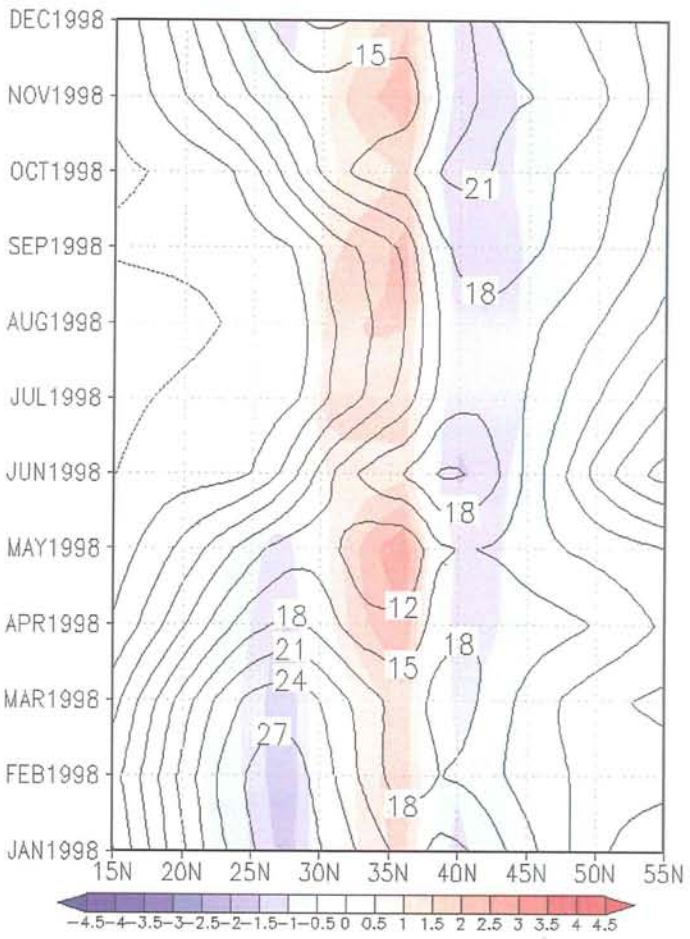

Fig. 5.6: Same with Fig. 5.5 but for ZM-FLQ experiment

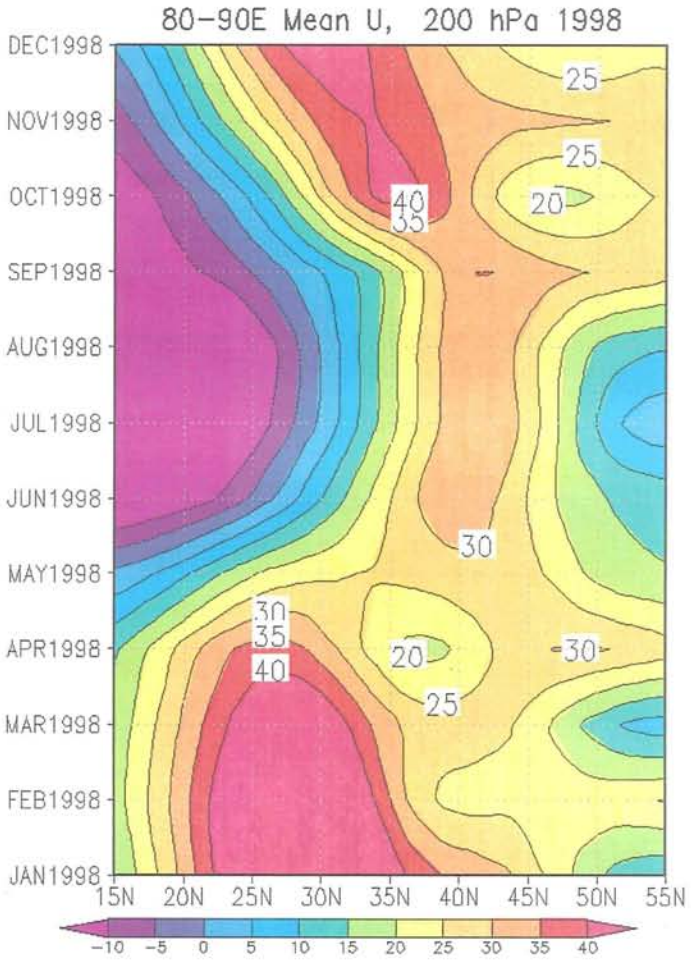

Fig. 5.7: Seasonal variation of zonal wind velocity (m sec^{-1}) at 200 hPa averaged between 80°E and 90°E.

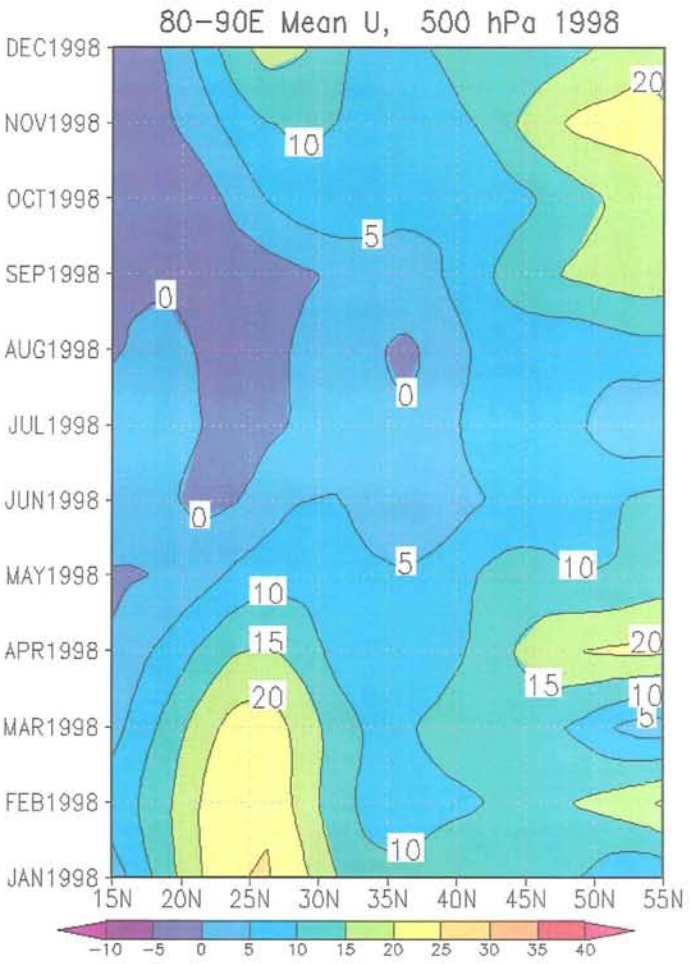

Fig. 5.8: Same with Fig. 5.7 but for 500 hPa.

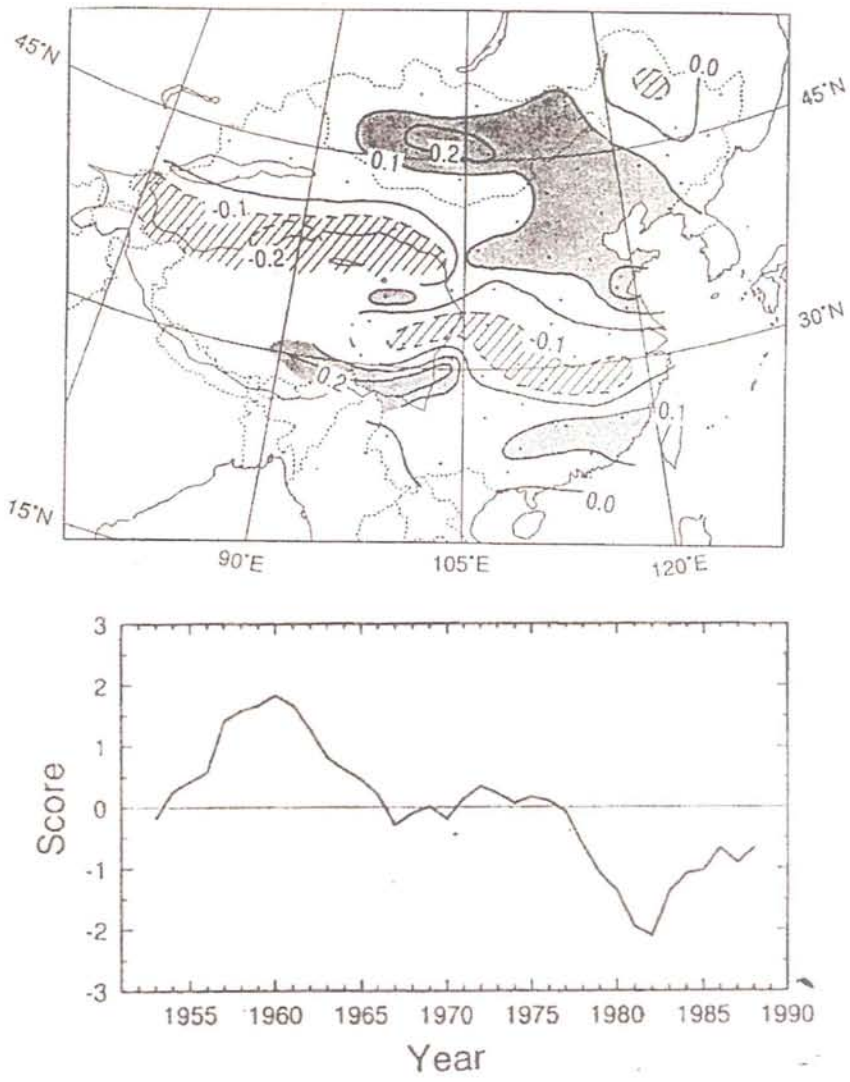

Fig. 5.9: Eigenvector pattern and score of first EOF (Empirical Orthogonal Function) of summer precipitation (From Yatagai and Yasunari, 1994)

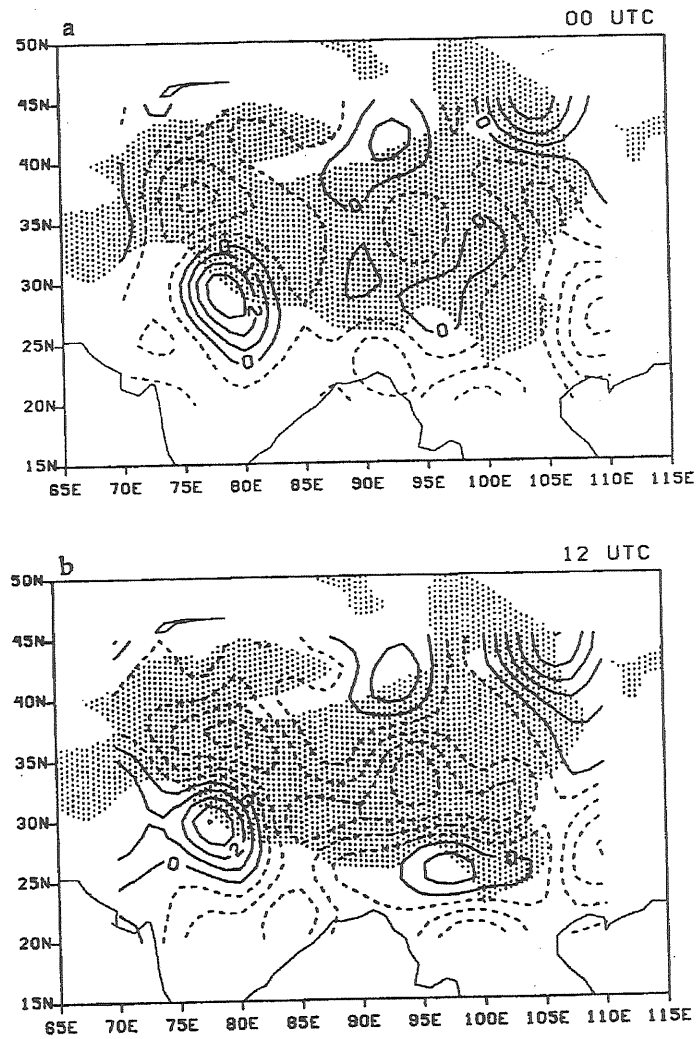

Fig. 5.10: Four-month mean vertical p velocity (hPa hr^{-1}, negative upward): (a) 0000 UTC, and (b) l200 UTC. (From Yanai and Li, 1994)

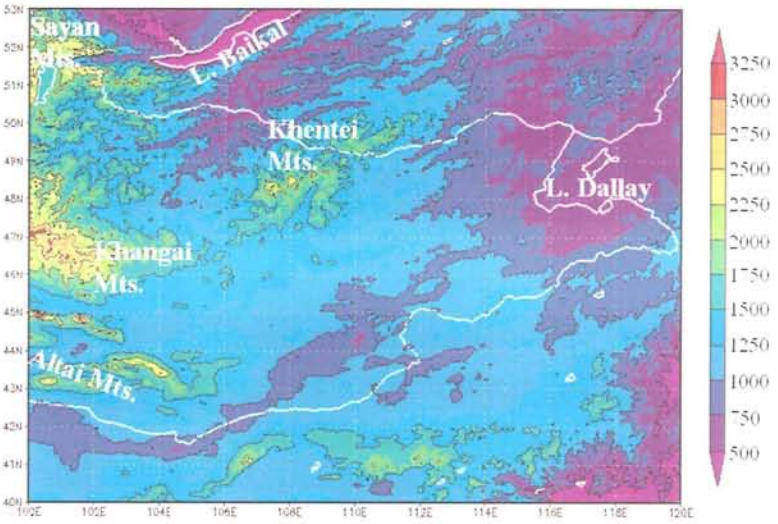

Fig. 5.11: Topography over eastern Mongolia.

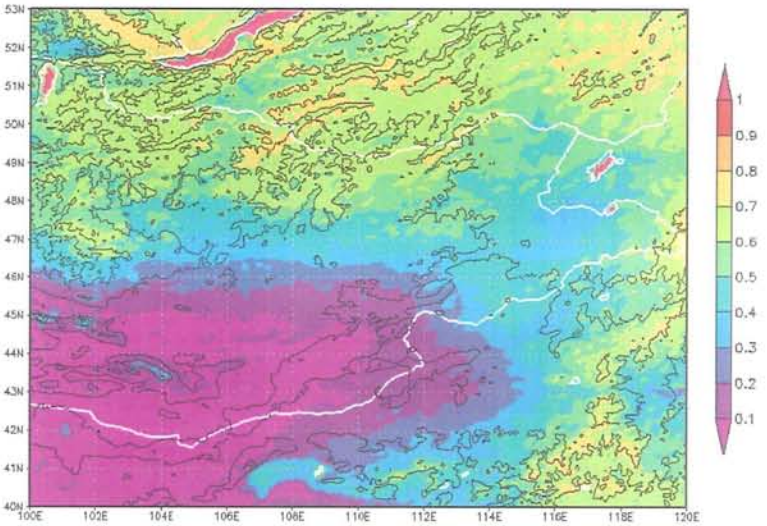

Fig. 5.12: Climatology NDVI distribution in middle July around northern China and Mongolia. Solid contours indicate topography in each 500 m.

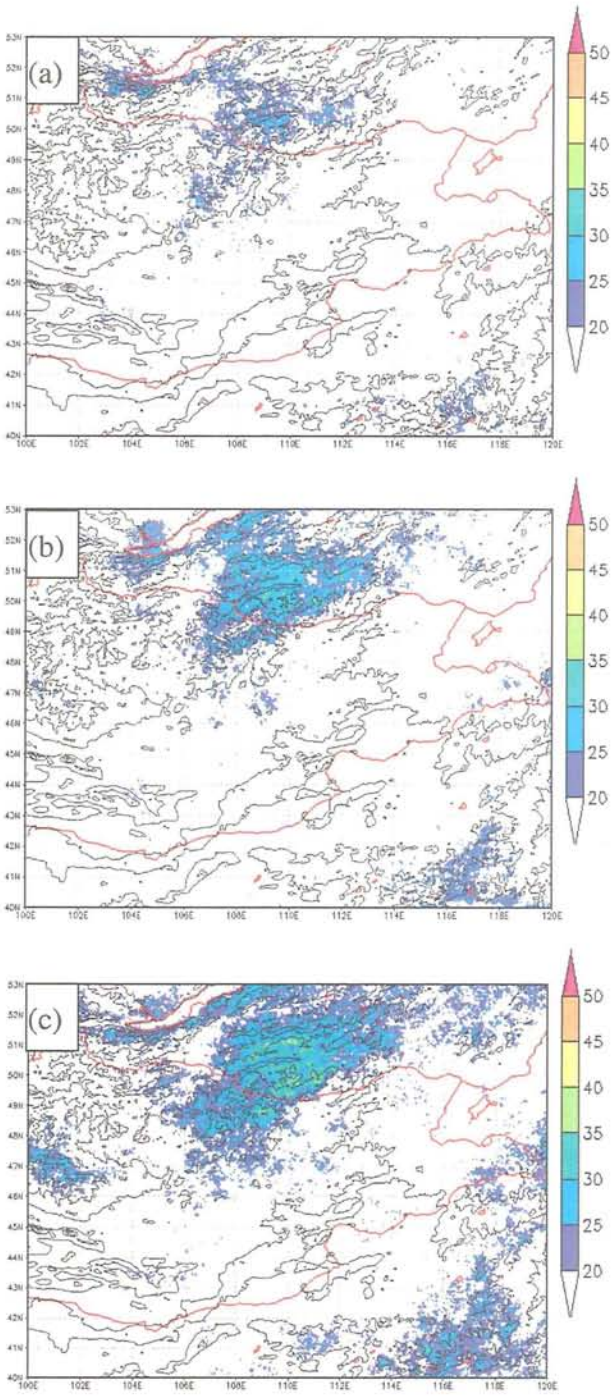

Fig. 5.13: Cloud frequency (%) at (a) 08 LT, (b) 10LT, (c) 12LT. Solid contours are drawn in each 500 m.

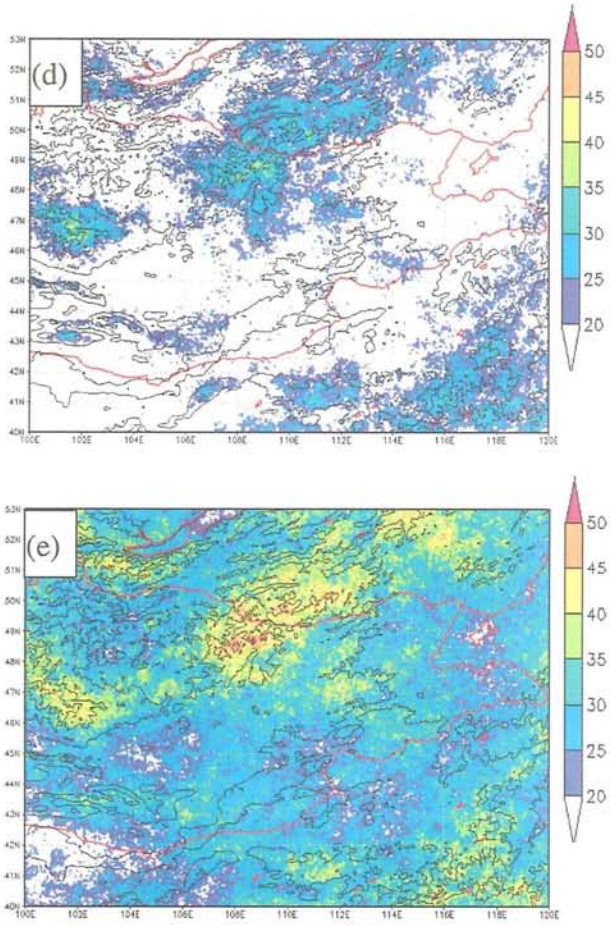

Fig. 5.13: Continued. (d) 14LT, (e) 16LT.

6. Conclusions

The formation mechanism of arid climate over northeastern Asia is investigated by RCM experiments. Before this study, rain-shadow effect by the TianShan Mountain is considered to be a major reason of the arid climate (Houghton, 1984; Hartmann, 1994; Shinoda, 2002). The LT-CTL experiment successfully simulates the arid region as a ten-year mean of precipitation. Rainfall distribution indicates the existence of rain-shadow by the TianShan Mountain. However, the simulation without the TianShan Mountain does produce an arid climate in almost same location. This fact indicates that the arid climate in northeastern Asia is formed even though rain-shadow effect is absent. Role of the TianShan Mountain is just to increase precipitation in upwind side, and the mountain does not affect the amount of precipitation in leeside where desert climate prevails. In general, precipitation systems, accompanied with synoptic disturbances passing through middle latitude Asia, provide abundant rainfall in northeastern Asia in warm season. However, rain band tends to weaken near northern periphery of the Tibetan Plateau, especially over the arid region, by a regional scale subsidence. Thus, precipitation hardly occurs over the desert region such as the Taklimakan and the Gobi deserts.

Sensitivity experiments with simple boundary conditions are carried out in order to clarify the cause of the subsidence appeared in northeastern Asia. The descending motion prevailing over the arid region is very prominent even when boundary condition of the model is assumed to be a time-independent zonal-mean condition. Arid area with less precipitation is also formed over north of the Tibetan Plateau in sensitivity experiment (ZM-CTL). Additionally, the prominent subsidence still persists in the experiment without condensation process in model physics (ZM-NoC). This indicates that diabatic heating process induced by condensation of water vapor is not always necessary to enhance the subsidence, since solar radiation heating contributes to most portion of the diabatic heating in ZM-NoC experiment. Thus, upward sensible heat flux from the plateau surface would be more efficient to drive the

subsidence, since surface of the plateau exists at an equivalent height of middle troposphere. The distinct subsidence over the arid region is formed when artificial diabatic heating is added over the Tibetan Plateau. Thus, the subsidence is caused by a diabatic heating over the plateau. The ZM-NoR experiment, in which radiation and condensation processes are turned off, reveals that vertical motion shows very small amplitude without diabatic heating indicating less importance of the mechanical effect of the Tibetan plateau.

Diabatic heating on the Tibetan Plateau is very affective to atmospheric circulation that leads to a generation of stationary wave which causes subsidence around the Tibetan plateau. Zonal wind speed, especially the latitudinal location of subtropical jet, determines horizontal direction of the stationary wave propagation. If subtropical jet locates in south to the heated region, the subsidence tends to prevail over southwest to the heat source. In general, subtropical jet runs north of the Tibetan Plateau in boreal summer when considerable aridity occurs in arid region. Stationary wave tends to propagate northward because subtropical westerly jet is being situated north of the plateau. Therefore, descending motion prevails over arid region in northeastern Asia, which consequently reduces amount of precipitation.

Acknowledgments

I would like to express special thanks to Prof. Fujio Kimura who has supported over all research activities in the University of Tsukuba. Additionally, I would very much appreciate his encouragements during my student time in Tsukuba, especially in first few years in graduate school. Many ideas on experimental setup in this study were raised at brainstorming with him both in personal and at seminars. Countless comments and suggestions are given from Prof. Hiroshi. L. Tanaka, Prof. Hiroaki Ueda, Prof. Yousay Hayashi, and Ken'ichi Ueno in University of Tsukuba and Prof. Tetsuzo Yasunari in Nagoya University, which greatly aid in proceeding analysis of this work. Appreciation extends to my colleagues Mr. Masayuki Hara of Frontier Research Center for Global Change and Dr. Osamu Okamura of Japan Ground Self Defense Force with whom I have shared much precious period discussing. Their advices and cooperation on the model setup, data processing, field observations, and encouragements were essential to achieve this work as well as my other studies in meteorology. I wish to express my thanks to the members of meteorological and climatological group of University of Tsukuba, especially Dr. Takao Yoshikane of Frontier Research Center for Global Change, Dr. Taichi Sasaki of Institute of Observational Research for Global Change, Dr. Yasunori Kurosaki of Meteorological Research Institute, Mr. Toru Yokotsuka of Japan Weather Association, Mr. Tetsuro Takagi of CRC corporation, for their encouragements not only teaching me the basis of meteorological data analysis. Part of satellite data analysis has been carried out in cooperation with Mr. Akira Hasegawa in the master's program in environmental sciences, University of Tsukuba. Data analysis and model setup are supported by Ms. Tomoe Kurokawa in Terrestrial environment research center, University of Tsukuba.

I feel very happy that I can continue meteorological research as a technician of CREST project since I gave up the graduate school in halfway. All of this work has been supported by the CREST project of Japan Science and Technology Agency (JST). Research environment in University of Tsukuba is mainly arranged by Prof. Michiaki Sugita. I would

like to express special thanks for his attentions and for giving me many opportunities participating field observations in Mongolia as well as employing me in CREST project. Without doubt, the experience of several field investigations in Mongolia was essential and indispensable for this study. The activity in Mongolia was carefully attended by RAISE project members, especially Prof. Jun Asanuma, Prof. Maki Tsujimura, and Prof. Tsutomu Yamanaka in University of Tsukuba, Dr. Sheng-Gong Li of JST, and Prof. Hiroyuki Iwasaki of Gunma University. Dr. Shin Miyazaki in University of Tokyo gave me many advices and suggestions on meteorological research in Mongolia and on this study. Field activities in Mongolia and many works in RAISE project are carefully supported by Ms. Yasuyo Sawaguchi of JST. I would like to thank to RAISE members for their encouragements.

Finally, I feel special thanks to my parents. They have continuously supported me before and after I left Tokamachi. Deepest and particular appreciations should be brought to my wife, Keiko. Her cooperation in data analysis and advices were essential for this study. I can summarize my study in aid with her supports in family and a lot of encouragements.

References

Adler, R.F., G. J. Huffman, A. Chang, R. Ferraro, P. Xie, J. Janowiak, B. Rudolf, U. Schneider, S. Curtis, D. Bolvin, A. Gruber, J. Susskind, P. Arkin and E. Nelkin, 2003: The Version-2 Global Precipitation Climatology Project (GPCP) Monthly Precipitation Analysis (1979 - Present). *J. Hydrometeorol.*, **4**, 1147-1167.

Arakawa, A. and W. H. Schubert, 1974: Interaction of a cumulus cloud ensemble with the large-scale environment, Part I. *J. Atmos. Sci.*, **31**, 674-701.

Armstrong, R. W. (Ed.), 1969: *Atlas of Hawaii.* University of Hawaii Press, Honolulu.

Batima, P. and D. Dagvadorj, 2000: Climate change and its impacts in Mongolia. JEMR Publishing, Mongolia, 227pp.

Bosilovich, M. G. and S. D. Schubert, 2002: Water Vapor Tracers as Diagnostics of the Regional Hydrologic Cycle. *J. Hydrometeor.*, **3**, 149–165.

Broccoli, A. J. and S. Manabe, 1992: The effects of orography on midlatitude northern hemisphere dry climates. *J. Climate*, **5**, 1181-1201.

Charney, J., 1975: Dynamics of deserts and drought in the Sahel. *Q. J. R. Meteorol. Soc.*, **101**, 193-202.

Chen S., Y. Kuo, P. Zhang and Q. Bai, 1991: Synoptic climatology of cyclogenesis over east Asia, 1958-1987. *Mon. Wea. Rev.*, **119**, 1407-1418.

Duan, A. M. and G. X. Wu, 2004: Role of the Tibetan Plateau thermal forcing in the summer climate patterns over subtropical Asia. *Clim. Dyn.*, in press.

Hartmann, D., 1994: *Global physical climatology.* Academic press. 411pp.

He, H., J. W. McGinnis, Z. Song and M. Yanai, 1987: Onset of the Asian summer monsoon in 1979 and the effect of the Tibetan Plateau. *Mon. Wea. Rev.*, **115**, 1966-1995.

Hoskins, B. J., 1996: On the Existence and Strength of the Summer Subtropical Anticyclones. *Bull. Amer. Meteor. Soc.*, **77**, 1287-1292.

Houghton, J. T., 1984: *The global climate.* Cambridge univ. press. 256pp.

Kalnay, E., M. Kanamitsu, R. Kistler, W. Collins, D. Deaven, L. Gandin, M. Iredell, S. Saha,

G. White, J. Woollen, Y. Zhu, A. Leetmaa, B. Reynolds, M. Chelliah, W. Ebisuzaki, W. Higgins, J. Janowiak, K.C. Mo, C. Ropelewski, J. Wang, Roy Jenne and Dennis Joseph 1996: The NCEP/NCAR 40-Year reanalysis project. *Bull. Amer. Meteor. Soc.*, **77**, 437-471.

Kurosaki, Y. and M. Mikami, 2002: Seasonal and regional characteristics of dust event in the Taklimakan Desert. *J. Arid Land Studies*, **11**, 245-252.

Lee S. H. and F. Kimura, 2001: Comparative studies in the local circulation induced by land-use and by topography. *Boundary-Layer Meteorol.*, **101**,157-182.

Liu, X. and Z.-Y. Yin, 2001: Spatial and temporal variation of summer precipitation over the eastern Tibetan plateau and the north Atlantic oscillation. *J. Climate*, **14**, 2896-2909.

Luo, H. and M. Yanai, 1984: The large-scale circulation and heat sources over the Tibetan Plateau and surrounding areas during the early summer of 1979. Part II: Heat and moisture budgets. *Mon. Wea. Rev.*, **112**, 966-989.

Manabe, S. and T. B. Terpstra, 1974: The effects of mountains on the general circulation of the atmosphere as identified by numerical experiments. *J. Atmos. Sci.*, **31**. 3-42.

Manabe, S. and A. J. Broccoli, 1990: Mountains and arid climates of middle latitudes. *Science*, **247**, 192-195.

Minoura, D., R. Kawamura and T. Matsuura, 2003: A Mechanism of the Onset of the South Asian Summer Monsoon. *J. Meteor. Soc. Japan*, **81**, 563-580.

Nakajima, T., M. Tsukamoto, Y. Tsushima, A. Numaguti and T. Kimura, 2000: Modeling of the radiative process in an atmospheric general circulation model. *Appl. Opt.*, **39**, 4869-4878.

Neuberger, H. and J. Cahir, 1969: *Principles of Climatology.* Holt, Rinehart and Winston, New York.

New, M. G., M. Hulme and P. D. Jones, 2000: Representing 20th century space-time climate variability. II: Development of 1901-1996 monthly terrestrial climate fields. *J. Climate*, **13**, 2217-2238.

Pielke, R. A., W. R. Cotton, R. L. Walko, C. J. Tremback, W. A. Lyons, L. D. Grasso, M. E. Nicholls, M. D. Moran, D. A. Wesley, T. J. Lee and J. H. Copeland, 1992: A comprehensive meteorological modeling system RAMS. *Meteorol. Atmos. Phys.*, **49**, 69-91.

Reynolds, R.W., N.A. Rayner, T.M. Smith, D.C. Stokes and W. Wang, 2002: An Improved In Situ and Satellite SST Analysis for Climate, *J. Climate*, **15**, 1609-1625.

Rodwell, M. J. and B. J. Hoskins, 1996: Monsoons and the dynamics of deserts. *Q. J. R. Meteorol. Soc.*, **122**, 1385-1404.

Sato, T. and F. Kimura, 2003: A two-dimensional numerical study on diurnal cycle of mountain lee precipitation. *J. Atmos. Sci.*, **60**, 1992-2003.

Sato, T., 2004: A funnel cloud and downburst over Mongolia on 2 July 2003. *Tenki*, **51**, 161-162. (in Japanese)

Sato, T. and F. Kimura, 2004: The impact of diabatic heating over the Tibetan plateau upon Northeastern Asia arid region. *Proceedings of the 6th International Study Conference on GEWEX in Asia and GAME.*

Sato, T., F. Kimura and A. Hasegawa, 2004: Cloud frequency in eastern Mongolia and its relation to the orography. *Proceedings of the 3rd International workshop on terrestrial change in Mongolia.*

Sato, T. and F. Kimura, 2005: Diurnal cycle of convective instability around the Central Mountains in Japan during the Warm Season. *J. Atmos. Sci.*, in press.

Shinoda, M., 2002: Sabaku to Kikou (Desert and Climate), Kisho books 014. Seizando Press. 169pp. (in Japanese)

Shukla, J. and Y. Mintz, 1982: Influence of land-surface evapotranspiration on the Earth's climate. *Science*, **215**, 1498-1501.

Takemi, T., 1999: Structure and evolution of a severe squall line over the arid region in northwest China. *Mon. Wea. Rev.*, **127**, 1301-1309.

Takemi, T. and T. Satomura, 2000: Numerical experiments on the mechanisms for the development and maintenance of long-lived squall lines in dry environments.

J. Atmos. Sci., **57**, 1718-1740.

Tanaka, H. L., N. Ishizaki and A. Kitoh, 2004: Trend and interannual variability of Walker, monsoon, and Hadley circulations defined by velocity potential in the upper troposhere. *Tellus*, **56A**, 250-269.

Trenberth, K. E., 1999: Atmospheric moisture recycling: Role of advection and local evaporation. *J. Climate*, **12**, 1368-1381.

Ueda, H., H. Kamahori and N. Yamazaki, 2003: Seasonal contrasting features of heat and moisture budgets between the eastern and western Tibetan Plateau during the GAME IOP. *J. Climate*, **16**, 2309-2324.

Walko, R. L., W. R. Cotton, M. P. Meyers and J. Y. Harrington, 1995: New RAMS cloud microphysics parameterization. Part 1: The single-moment scheme, *Atmos. Res.*, **38**, 29-62.

Wang, B. and LinHo, 2002: Rainy season of the Asian-Pacific summer monsoon. *J. Climate*, **15**, 386-398.

Warner, T., 2004: *Desert Meteorology.* Cambridge univ. press. 595pp.

Wu, G. and Y. Zhang, 1998: Tibetan plateau forcing and the timing of the monsoon onset over South Asia and the South China Sea. *Mon. Wea. Rev.*, **126**, 913–927.

Xue, Y. and J. Shukla, 1993: The influence of land surface properties on Sahel climate: Part I. Desertification. *J. Climate*, **6**, 2232-2245.

Yanai, M. and C. Li, 1994: Mechanism of heating and the boundary layer over the Tibetan Plateau. *Mon. Wea. Rev.*, **122**, 305-323.

Yatagai, A. and T. Yasunari, 1994: Trends and Decadal-Scale Fluctuations of Surface Air Temperature and Precipitation over China and Mongolia during the Recent 40 Year Period (1951-1990). *J. Meteor. Soc. Japan*, **72**, 937-957.

Yatagai, A. and T. Yasunari, 1995: Interannual Variations of Summer Precipitation in the Arid/semi-arid Regions in China and Mongolia: Their Regionality and Relation to the Asian Summer Monsoon. *J. Meteor. Soc. Japan*, **73**, 909-923.

Yoshikane, T., F. Kimura and S. Emori, 2001: Numerical study on the Baiu Front genesis by

heating contrast between land and ocean. *J. Meteor. Soc. Japan*, **79**, 671-686.

Yoshino, M., 1991; Wind and rain in the desert region of Xinjiang, China. *J. Arid Land Studies*, **1**, 1-15 (in Japanese with English abstract).